WORCESTER POLYTECHNIC INSTITUTE – DEPARTMENT OF CHEMICAL ENGINEERING
100 INSTITUTE ROAD, WORCESTER, MA 01609

Effect of pH on polyelectrolyte multilayer formation and growth factor release

by

Claire SALVI

A thesis submitted to the faculty of
WORCESTER POLYTECHNIC INSTITUTE
In partial fulfillment for the requirement for the Degree of
Master of Science
In
Chemical Engineering
May 2015

Claire SALVI

Dr Amy M. PETERSON,
Advisor

Dr David DiBiasio,
Head of the Department

Acknowledgements

As two years of work are coming to an end, when all has been said and done, I would like to thank the following people for everything they have done, sometimes unknowingly, in order for me to complete this thesis:

Professor Amy M. Peterson for her dedicated guidance, help and support, as well as for having taken me under her wing and welcoming me to her lab during this research project,

All members of the Functional Surfaces and Interfaces Lab, with special thanks to Anthony D'Amico, Lv Xuejian and Huilin Yang for their keen advices and cheerfulness,

Professor Christopher R. Lambert for use of the goniometer and Aung Lynn for training on the goniometer,

Professor David S. Adams for use of the incubator,

Professor Nancy A. Burhnam for use of the AFM and Gawain Thomas for training on the AFM,

Worcester Polytechnic Institute (WPI) chemical engineering faculty and staff members, especially Felicia Vidito and Tiffany Royal for their constant help,

The Ecole Nationale Supérieure des Industries Chimiques (ENSIC school, Nancy, France) for giving me the chance to participate in their partnership program with WPI,

And last but not least, all of my friends and relatives for their kind support and patience during these past two years.

Abstract

Because of its high specific strength, durability, and biocompatibility, titanium is a widely used material for orthopedic implants. However, its insufficient binding with the surrounding bone tissue regularly leads to stress shielding, bone resorption and implant loosening. A promising solution to improve adhesion is to modify the implant surface chemistry and topography by coating it with a protein-eluting polyelectrolyte complex.

Bone morphogenetic protein 2 (BMP-2), a potent osteoconductive growth factor, was adsorbed onto the surface of anodized titanium, and polyelectrolyte multilayer (PEM) coatings prepared from solutions of poly-L-histidine (PLH) and poly(methacrylic acid) (PMAA) were built on top of the BMP-2. The effect of solution pH during the deposition process was investigated. High levels of BMP-2 released over several months were achieved. Approximately 2 μg/cm² of BMP-2 were initially adsorbed on the anodized titanium and a pH-dependent release behavior was observed, with more stable coatings assembled at pH = 6-7. Three different diffusion regimes could be determined from the release profiles: an initial burst release, a sustained release regime and a depletion regime.

Mass adsorption monitoring using quartz crystal microbalance with dissipation monitoring (QCM-D) showed that PLH was adsorbed in greater quantities than PMAA, and that more mass was adsorbed per bilayer as the number of bilayers grew. Moreover, the pH of the water used during the rinsing step significantly impacted the composition of the multilayer.

Atomic force microscopy (AFM) and contact angle analysis (CAA) were used to determine the topography and surface energy of the PEMs. No visible change was observed in surface morphology as the assembly pH was varied, whereas the surface energy decreased for samples prepared at more basic pH. These variations indicate that the influence of the initial BMP-2 layer can be felt throughout the PEM and impact its surface structure.

Table of contents

List of symbols and abbreviations

ACS	American Chemical Society
AFM	Atomic Force Microscopy
BMP	Bone Morphogenetic Protein
C	Mass sensitivity constant
C_0	Initial concentration
C_S	Solubility
D	Fickian diffusion coefficient or QCM-D dissipation
E	Spring stiffness
ELISA	Enzyme Linked Immune Sorbent Assay
f	Frequency
FBAR	Film Bulk Acoustic Resonators
FDA	Food and Drug Administration
K	Constant reflecting the system design variables
LbL	Layer by Layer
m	Mass
M	Molar concentration (ie molarity)
M_n	Number average molecular weight
M_t	Total/Cumulative mass at time t

n	Overtone number or power law coefficient or amount of moles
OECD	Organization for Economic Co-operation and Development
p	Number of drops
PAA	Poly(Acrylic Acid)
PAH	Polyallylamine Hydrochloride
PBS	Phosphate Buffered Saline
PCBS	Poly{1-[*p*-(3′-carboxy-4′-hydroxyphenylazo)benzenesulfonamido]-1,2-ethandiyl}
PDADMAC	Poly(diallyldimethylammonium chloride)
PDGF	Platelet-Derived Growth Factor
PEI	Polyethyleneimine
PEM	Polyelectrolyte Multilayer
PGA	Poly(L-Glutamic Acid)
PLH	Poly-L-Histidine
PLL	Poly-L-Lysine
PMAA	Poly(Methacrylic Acid)
PNIPAM	Poly(N-isopropylacrylamide)
PSS	Poly(sodium 4-styrenesulfonate)
QCM	Quartz Crystal Microbalance
QCM-D	Quartz Crystal Microbalance with Dissipation monitoring
R^2	Coefficient of determination

t	Time
t_q	Quartz crystal thickness
TGF	Transforming Growth Factor
V	Volume
VEGF	Vascular Endothelial Growth Factor
W_a	Work of adhesion
wt. %	Weight percent

Greek letters

ε	Material strain
η	Material viscosity
γ_S	Surface free energy of a solid
γ_L	Surface free energy of a measuring liquid
γ_{SL}	Surface free energy at the solid/liquid interface
ρ_q	Quartz crystal density
σ	Material stress
θ	Contact angle

List of figures

List of tables

I. Introduction

Among all specialties represented in the surgery field, orthopedics, or orthopedic surgery, can be considered as one of the oldest. This discipline is centered on the treatment of all pathologies affecting bones and the musculoskeletal system, including the repairing of fractures and malformations, the treatment of infections and joint pains, and the implementation of artificial implants. Implanted devices are used to relieve or replace deficient articulations such as knees, hips, and the spinal cord. In 2012, in the United States alone, 1.16 million hip and knee replacements were performed, a number that has doubled since 1995 and is expected to continue increasing.[1] One of the major concerns regarding implants is to ensure their long term performance as they become more common among the population, and as the average life expectancy steadily increases. Most joint replacements are rated for approximately one million cycles, which amounts to fifteen to twenty years depending on patient activity. Nonetheless, more than 100,000 revisions to knee and hips implants were performed in 2012, which roughly represents a 10% revision rate per year. This revision rate has been overall stable since 1994.[2,3]

One of the leading causes of implant revision is limited integration with the surrounding bone tissue, either because of poor adhesion and growth of bone cells and tissue on the scaffold or because of micro-motions inhibiting the biological integration process.[4] Significant advances have been achieved over the past few decades; however, the complex interactions taking place at the bone-implant interface are not yet fully understood nor controlled. A promising solution for improving osseointegration exists in the form of drug-eluting coatings. Substances that can be released from these systems include drugs such as antibiotics or pain killers, as well as growth factors such as bone morphogenetic proteins. Bone morphogenetic protein 2 (BMP-2), for example, is known for its potent osteoinductive effect, which enhances osteoblast differentiation and stimulates extracellular matrix mineralization.[2] However, due to the long period of time required for these phenomena to take place after a replacement surgery, the release of BMP-2 should occur in a controlled manner so as to optimize its effect on the surrounding tissue.

The enhanced biocompatibility and stability of polyelectrolyte multilayers (PEMs), along with their capacity to control the release of a loaded molecule, make them suitable candidates to be used as implant coatings along with BMP-2. Moreover, these systems are extremely versatile, as their properties can be tuned by adjusting parameters such as temperature, salt concentration, electrical environment, ultrasound, and pH.[5–10] However, the flexibility of PEMs can also be considered as a weak point, since each PEM system will behave in an individual way in response to identical stimuli. In this regard, a careful investigation of the combined influences of pH, PEM structure and PEM properties is required in order to fully understand the mechanisms at work for a given system. The aim of this work is to perform such a study and use that information to tailor coatings for implants in a controlled and efficient manner.

In this research, PEM assembly pH has been studied in order to investigate its impact on the structure and properties of the resulting coating. The PEM considered was made of an initial layer of BMP-2 adsorbed on anodized titanium and covered with five bilayers of PLH/PMAA. By varying the solutions pH between 4.0 and 8.0, the following aims have been pursued:

1. Investigate the effects of the PEM assembly pH on growth factor release from the multilayer. It is supposed that the assembly pH of the PEM system influences its BMP-2 release in a controlled way, thus making it suitable as an implant coating candidate.
2. Characterize the effect of the PEM assembly pH during the multilayer formation. The working hypothesis, based on literature review, is that the assembly pH of the PEM system impacts its internal structure during the buildup process as it affects the electrostatic interactions holding together the different layers.
3. Demonstrate the impact of the PEM assembly pH on the multilayer surface. It is postulated that the differences in internal structure caused by the assembly pH influence the PEM surface properties.

After providing sufficient background information, the research performed during this thesis project in order to confirm or refute these hypotheses is presented and discussed.

II. Background information

In medicine, an implant is defined as "an object or material inserted or grafted into the body for prosthetic, therapeutic, diagnostic or experimental purposes".[11] The first applications of such devices have been shown to go back as far as the ancient Egyptian era, where people used fake toes made out of wood or papier mâché. A British research group led by Jacqueline Finch demonstrated that these early external prostheses did not merely fulfill an aesthetic role, but significantly eased the motion and comfort of walking.[12] However, it was not until the end of the nineteenth century that the first functional internal implants appeared. Unlike fake limbs, these devices were placed directly into the body, which may explain their late development when compared to external implants, as their development required a more advanced knowledge of human anatomy and the act of surgery. The German surgeon Themistocles Gluck is recognized as the first scientist to extensively research internal implants. Gluck reported successful operations using ivory joints as early as 1890.[13] Afterwards, research in this domain increased, with important contributions being brought by the Judet brothers, who conceived of the first total hip replacement to be widely used in surgical acts in 1946, and Sir John Charnley, who designed a modern version of a total hip implant in 1962. Models of the Charnley implant are still in use today.[14]

Since the 1970's, the number of operating procedures related to joint replacements have been steadily increasing. The Organization for Economic Co-operation and Development (OECD) reported an increase of 30% in hip replacements and nearly 50% in knee replacements between 2000 and 2011. In the United States alone, the number of both procedures more than doubled during that period of time (see appendix 1).[15] More than 1.55 million knee replacements, hip replacements and spinal fusions were performed in that country in 2012, which represented almost 20% of all surgeries registered that year and an increase of 9% as compared to 2011.[16] All three of these medical acts have been consistently ranked in the top ten most performed procedures as well as the top ten most expensive procedures for several years (see appendix 2).[1,17]

Although the field of joint replacement has experienced significant advancements during the past century, there are still fundamental issues related to the aging of joint replacements. Caton and Papin pointed out that several studies around the world reported a durability rate of 90% after fifteen years for hip implants. This rate decreased to 85% after 25 years and about 75% after thirty-five years.[14] Overall, an implant lifespan will range from ten to thirty years depending on its materials, the patient physical activity and their weight, with the average value hovering between fifteen and twenty years. Other factors can significantly decrease an implant lifespan, such as nosocomial infections, which cause 1 to 5% of all primary joint replacement failures, inappropriate mechanical load, and implant wear and fatigue failures at the bone/implant interface.[3] In the United States alone, roughly 10% of all joint replacements are revision surgeries caused by one of these problems.[18]

Implant wear and fatigue failures are especially problematic, as they create micro-motions between the bone and the implant. Not only do these micro-motions accelerate the degradation of the joint replacement by creating debris that leads to inflammatory reactions and potential poisoning, but they have also been shown to increase undesirable physiological responses such as bone resorption. Moreover, if the micro-motions are due to a poor initial fixation of the implant, the device is more likely to fail early, which defies its original purpose and may lead to more pain for the patient.[3] Research has thus been focused on ways of increasing the early osseointegration of implants in order to increase their lifespan and thus decrease the number of revision surgeries. The solutions proposed to achieve this goal include radiation therapy, bone marrow grafting or the simultaneous use of demineralized bone matrix associated with the implant, and local delivery of one or more biologics such as growth or differentiation factors to the injury site.[4,19] Research in this domain has notably reported the use of vascular endothelial growth factor (VEGF), fibroblast growth factors (FGFs), transforming growth factors (TGFs), mitogenic platelet-derived growth factor (PDGF) and bone morphogenetic proteins (BMPs). [20–24]

BMPs play a key role in tissue formation throughout the body; among them BMP-2 has been approved by the American Food and Drug Administration (FDA) and extensively used in controlled release application as it enhances osteoblast differentiation as well as bone extracellular matrix

mineralization.[2] Nonetheless, current BMP-2 delivery vehicles such as injections or implantable carriers have been shown to cause a series of adverse side effects such as pain, osteolysis or a greater risk of developing cancer cells, as well as suboptimal bone tissue regeneration, all because of the large quantities of growth factor suddenly released into the body.[23,24] A controlled, physiological release of BMP-2 is thus required in order to prevent these side effects. One option is a growth factor-eluting coating applied onto the surface of the implant. Various designs have been proposed such as drug loaded nanoparticles immobilized on the implant surface,[25] BMP-2 infused hydrogels,[26] plasma-induced surface functionalisation,[27] or immobilization on the titanium surface modified with heparin or silk proteins.[28,29] The use of polyelectrolyte layer-by-layer (LbL) complexes however has been one of the most promising options.

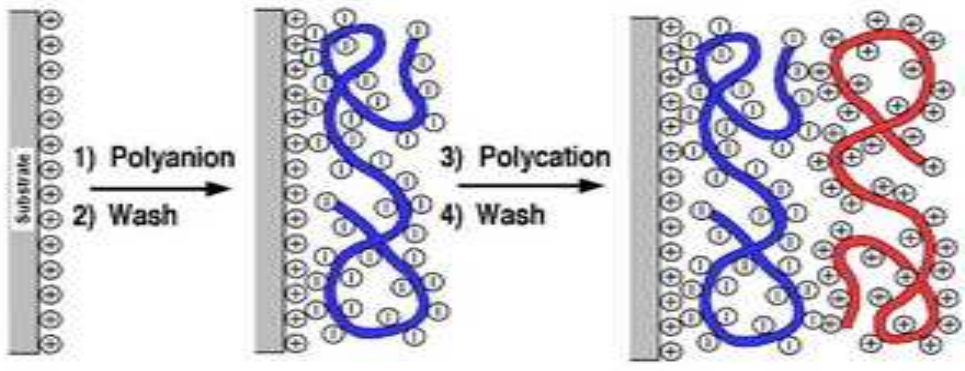

Figure 1: Principle of PEM formation

Polyelectrolytes are polymers with ionically dissociable repeat units. These groups can be positively charged for polycations, negatively charged for polyanions, or including both positive and negative charges for polyampholytes. Completely dissociated ionic groups are representative of strong polyelectrolytes, whereas there is a pH-dependent probability that any one ionic group will be dissociated on weak polyelectrolytes. The electrostatic interactions between the different charged groups can lead to the formation of polyelectrolyte complexes, for example by alternating layer by layer adsorption of a polycation and a polyanion (Figure 1). This specific structure, called a PEM, can be designed as a thin film or as capsules, thus allowing for a large variety in system design. Moreover, numerous studies have reported that PEMs show excellent biocompatibility.[30–32] As a result, these

systems have been used in numerous applications such as cell transfection or differentiation,[33,34] obtaining of nano-patterned surfaces,[35,36] design of a superhydrophobic surface,[37] functionalization of living cells,[38] or delivery systems for biologically relevant molecules including DNA,[39] antibiotics and anti-inflammatory drugs, [32,40,41] or growth factors.[20,42–44]

The versatility of PEM properties adds to the attention they draw as potential materials for controlled drug delivery. Over the past decade, several reviews have focused on how stimuli such as temperature, electric or magnetic fields, salt or sugar concentration can impact PEM permeability, thickness, swelling behavior, drug loading capacity, surface roughness or cell adhesion.[5,45–49] Further control over the drug release from these systems can be achieved by either cross-linking the different layers[50–53] or including nanoparticles in its structure.[20,54] Nonetheless, among all of these parameters, pH is one of the most interesting. For example, the work of Antipov et al. showed that the permeability of PEM capsules could be tuned by changing the external pH, thus allowing drug loading during the open state, transportation and storage during the closed state, and finally drug release by switching to an open state once again.[55–57] Research in this field has since then been booming. The pH-induced conformational changes and swelling transitions have been investigated, and the control over their reversibility achieved by pH-tuning has been repeatedly confirmed.[58–60] Similarly, pH-induced drug release from PEM was extended to films, which showed that both drug diffusion and PEM degradation were participating in the release process.[61,62] Large molecules such as BMP-2 and other growth factors were sustainably eluted from these coatings, and the resulting systems displayed a great stability.[21,53,61] Finally, Thompson et al. showed that the assembly pH was as important as the external pH in determining PEM properties such as elasticity and cell adhesion.[63]

Peterson et al. reported similar observations for another BMP-2 eluting PEM. This particular system consisted of a BMP-2 layer adsorbed on top of a titanium substrate and covered with several multilayers made of poly-L-histidine (PLH) and poly(methacrylic acid) (PMAA) (Figure 2). Sustained release of BMP-2 was observed for several weeks;[44] however, adjusting the deposition solution pH to pH = 6 during the PEM formation greatly increased the eluted amount of growth factor.[64] The work presented in this thesis aimed to investigate this last finding by expanding the range of assembly pH

values at which this particular system was built and studying its impact on different PEM properties, including the amount of BMP-2 released, the mass and structure of each layer, and the resulting surface properties. The final purpose of this research was to obtain a better understanding of the relationships linking the assembly pH, the PEM structure, and its resulting properties in order to design a tunable BMP-2 eluting system that could be efficiently used as an implant coating to enhance osseointegration.

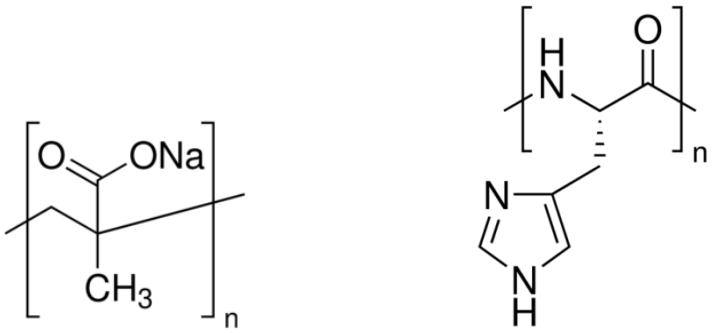

Figure 2: Chemical structure of PMAA (left) and PLH (right)

III. Experimental section

1. Materials

Titanium foil (99.5% metal basis, 0.25 mm thick) and titanium wire (99.7% metal basis, 0.25 mm in diameter) were purchased from Alfa Aesar. Poly(methacrylic acid, sodium salt) solution (PMAA, M_n ~ 5400, 30 wt.% in water), poly-L-histidine hydrochloride (PLH, molecular weight ≥ 5000), phosphate buffered saline (PBS, pH = 7.4), sodium hydroxide anhydrous pellets (≥ 98%), hydrochloric acid (ACS, reagent 37%) and sulfuric acid (ACS, reagent 95-98%) were obtained from Sigma Aldrich. Recombinant human bone morphogenetic protein 2 (BMP-2) as well as human BMP-2 enzyme linked immune sorbent assay (ELISA) development kits were acquired from Peprotech.

2. Titanium plates preparation

Titanium foil was cut into 1x1 cm² or 2x2 cm² plates. Each piece was soaked for at least one minute in 1 M hydrochloric acid in order to remove the natural oxide layer covering their surfaces. The plates were then rinsed with deionized water, ethanol, acetone, and water in this specific order so as to remove contaminants. They were then anodized in a 165 g/L sulfuric acid solution at a potential of 30 V for five minutes and rinsed afterwards with deionized water. The cathode was made of wrapped titanium wire whereas the anode consisted of the plate to be anodized connected to the power source with another titanium wire (Figure 3). Under those conditions, the pore sizes of the titanium dioxide surface range from 40 to 200 nm in diameter.[61]

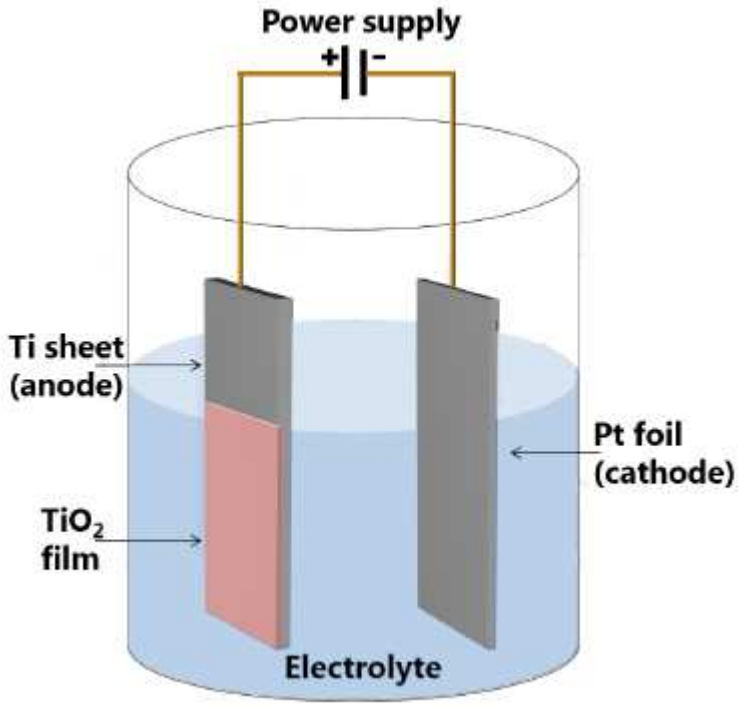

Figure 3: General scheme of an electrochemical cell used to produce TiO_2 films by anodization of Ti. The actual setup used in the experiment presented in this report consisted in wrapped titanium wire instead of a platinum foil.[65]

3. Build up of polyelectrolytes multilayers

Each anodized titanium plate was immersed in a 100 μg/mL BMP-2 in water solution for 15 minutes, during which time the BMP-2 adsorbed to the anodized titanium surface. After the deposition of this preliminary layer, the plates were rinsed three times in deionized water and the actual polyelectrolyte multilayer was built on top of it as follows. First, the plates were immersed in a 1 mg/mL PMAA in water solution for 15 minutes, after which they were rinsed three times in deionized water in order to remove loosely adsorbed polymer from the surface. They were then immersed in a 1 mg/mL PLH in water solution and once again left to adsorb for fifteen minutes before being rinsed three times in deionized water, thus concluding the formation of the first polyelectrolyte bilayer (Figure 4). This process was repeated until five PMAA/PLH bilayers (ten layers total) were obtained.

Peterson et al. showed that this resulting film was thick enough for an efficient sustained release of BMP-2.[44]

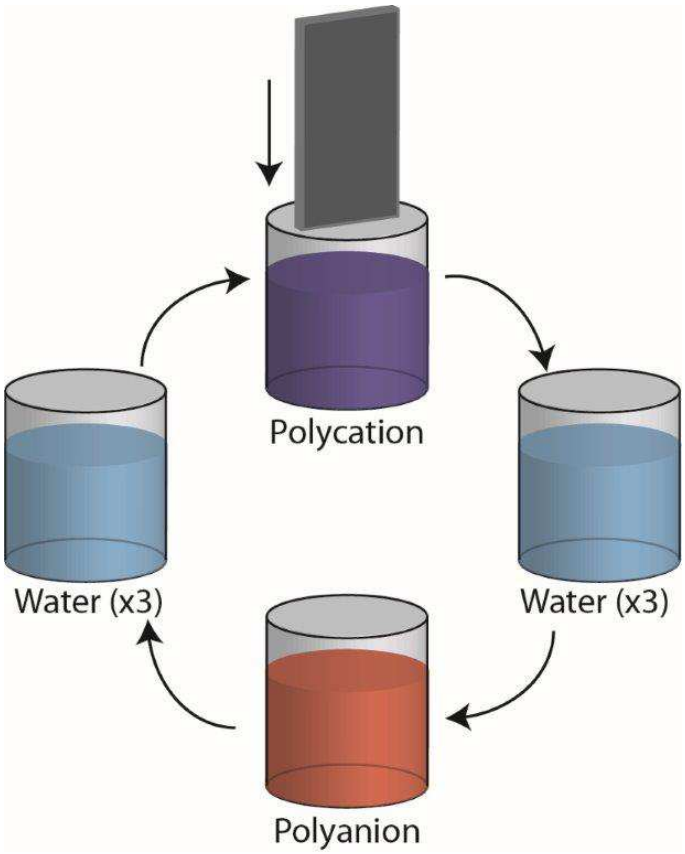

Figure 4: Scheme of the layer-by-layer formation of polyelectrolyte multilayers.[64] PMAA is the polyanion and PLH is the polycation.

For a given multilayer build-up, the PMAA and PLH solution as well as the water used for rinsing were all adjusted to the same pH using hydrochloric acid solutions (1 M and 0.1 M) and sodium hydroxide solutions (1 M and 0.1 M). Plates were prepared using solutions adjusted to pH 4.0, 5.0, 6.0, 7.0 and 8.0 in order to study the impact of this parameter on the BMP-2 release and the coating structure. Monitoring of the pH adjustment showed that the concentration of sodium/chloride ions added to the solutions was far less than 10^{-6} M; therefore, the influence of ions on polyelectrolyte conformation and resulting PEM structure was deemed negligible. All multilayers were prepared at room temperature (approximately 22 °C).

4. Growth factor release study

For each pH condition, the growth factor release study was conducted on five different samples, each sample consisting of a 1x1 cm² plate that was coated with solutions adjusted to that particular pH. After immersing them in PBS, the plates were incubated at 37 °C. Aliquots of 1 mL were regularly sampled after 1, 2, 4 and 8 hours, and after 1, 2, 3, 4, 7, 10, 14, 17, 21 and 25 days. All aliquots were immediately frozen at -30 °C after sampling and replaced with an equal volume of PBS. At the end of a release study the plates were rinsed first with 0.5 mL of a 0.1 M hydrochloric acid solution and then with 0.5 mL of a 0.1 M sodium hydrochloride solution in order to remove all leftover BMP-2 on the anodized titanium surface by breaking all electrostatic interactions between the PEM and substrate. The resulting 1 mL aliquot was then adjusted to pH = 7.4 with hydrochloric acid and sodium hydroxide solutions in order to match the pH of the previous aliquots (consisting primarily of PBS), and immediately frozen at -30 °C.

In order to define the impact of the assembly pH on the release of BMP-2 from the PEM samples, the amount of BMP-2 eventually reaching the surrounding PBS medium was quantified using a sandwich ELISA. This technique aims to detect antigens presented by the sample and is performed in a series of five main steps (Figure 5). First, a known quantity of capture antibody is adsorbed on a plate and any non specific binding sites are blocked to avoid cross-reactions. Then, the sample containing the antigen of interest is added so that it can binds to the capture antibody. The third step consists of adding a detection antibody that will also link to the sample, which will then become “sandwiched”. Non specific sites on the detection antibody are afterward linked to a third kind of antibody which present an enzyme. Finally, a chemical is added that will be converted by the enzyme into a detectable signal, usually by using colorimetry or fluorescence.

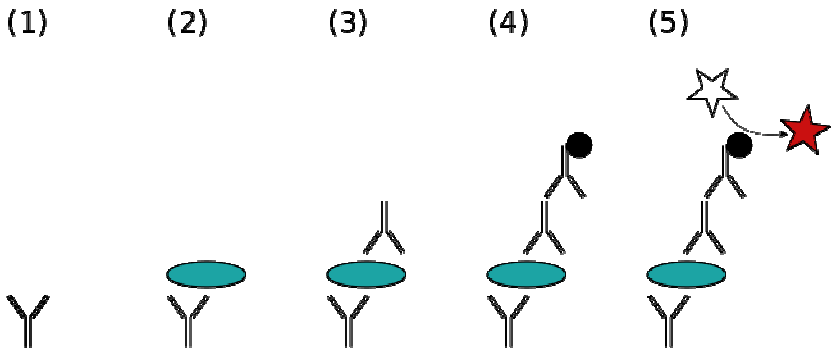

Figure 5: Principle of a sandwich ELISA. 1) Capture antibody adsorbed on surface, 2) Sample with antigen linked to capture antibody, 3) Detection antibody linked to antigen, 4) Enzyme linked antibody bound to detection antibody, 5) Substrate converted by enzyme into detectable form.

ELISA was performed in accordance with the instructions provided with the development kit. Aliquots were thawed and brought to room temperature before use, and dilutions ranging from 1/8 to 1/32 were selected in order to obtain results within the specified concentration limits for the ELISA protocol. Color monitoring of the ELISA plates was performed using a Perkin-Elmer Victor^3 multilabel reader with a 405 nm filter and a 650 nm correction filter.

5. Analysis of the coatings surface

a. Layer-by-layer mass monitoring

The amount of polyelectrolyte adsorbed on the plate surface for each layer was monitored for several pH conditions using a Q-Sense E4 quartz crystal microbalance with dissipation monitoring (QCM-D, Biolin Scientific). Briefly, QCM-D uses a quartz crystal resonator that oscillates at its fundamental frequency by piezoelectric effect in the absence of any perturbation. However, if mass is adsorbed or desorbed on the resonator surface its oscillating frequency will change, thus allowing for these variations to be tracked in real time. Moreover, if the frequency shift is coupled to dissipation monitoring, (which is to say the evolution of the system damping) as it is the case for QCM-D, information related to the sample viscoelasticity can be collected. As a consequence, this method has been increasingly used to determine film thickness and molecular affinity to surfaces in gas and liquid environments.[66–68]

Titanium plated QCM-D sensors were used to represent the actual titanium plates. Given the cost of manufactured BMP-2 and the amount of growth factor solution required to run through the QCM-D for 15 minutes to form a layer, the initial layer of BMP-2 was replaced by an extra layer of PLH. This first layer was made by running a 1 mg/mL pH-adjusted PLH in water solution through each QCM-D module, and then rinsing it by running the corresponding pH-adjusted deionized water for ten minutes.

The multilayer buildup was performed by first running a 1 mg/mL pH-adjusted PLH in water solution through each QCM-D module for fifteen minutes, then rinsing it with the corresponding pH-adjusted deionized water for ten minutes. The second layer was then adsorbed by running the 1 mg/mL PLH in water solution for fifteen minutes and rinsing it again afterward with water for ten minutes, thus leading to the formation of the first bilayer. This procedure was repeated until five bilayers (ten layers total) had been formed on top of the initial PLH layer. The QCM-D data were acquired using the software Q-Soft and treated with the software Q-Tools. For stiff thin films such as PEMs, the Sauerbrey equation can be used to linearly relate changes in frequency and mass:

$$\Delta m = -\frac{C}{n}.\Delta f \qquad (1)$$

In this equation, m is the adsorbed mass, f the resonant frequency, n the overtone number and C the mass sensitivity constant which in this case was equal to 17.7 ng/(cm^2.Hz). The validity of the Sauerbrey equation for this particular PEM system will be discussed in detail in section (V.4).

The impact of the rinsing water pH on the PEM was investigated by reproducing the same experiment while using regular (and not pH-adjusted) deionized rinsing water in between each polyelectrolyte adsorption step.

b. Contact angle analysis

Contact angle analysis was performed on 2x2 cm² titanium plates coated with BMP-2 and five PMAA/PLH bilayers using a contact angle goniometer (Ramé-Hart). Plates were prepared at pH 4, 5, 6, 7 and 8 as described previously. For each condition, several 2 µL droplets of deionized water,

glycerol, formamide or diiodomethane were dropped onto the corresponding plate and the resulting contact angles were measured using the software DropImage. When switching to a different liquid, the plates were rinsed three times with deionized water, dried with nitrogen and left to dry overnight beforehand.

The surface energy of each plate was determined from the contact angle measurements using the Owens-Wendt theory, which identifies the polar and dispersive contributions to the global surface energy.[69]

c. Atomic force microscopy

The surfaces of 2x2 cm² titanium plates prepared in the same manner as those used in contact angle analysis were imaged using an atomic force microscope (AFM, Nanosurf NaioAFM) in contact mode. Briefly, atomic force microscopy is a high resolution scanning probe technique using a cantilever with a sharp tip at its end that comes into contact with the sample surface. As the tip scans the sample, it is deflected by the asperities on the surface. This deflection is detected by a laser beam reflecting onto the probe and into a grid of photodiodes (Figure 6). This signal is then converted to an image. Piezoelectric elements located either in the sample stage or the cantilever holder constantly adjust the tip-to-sample distance through a feedback loop so as to maintain a constant pressure force and avoid breakage of the cantilever. Contact mode is capable of detecting features ranging from a hundred micrometers to a few nanometers as well as functionalizing surfaces, tracking living cells behaviors or even measuring adhesion forces [70,71]

Images presenting discrepancies such as scratches or unusual blobs of adsorbed polymers were discarded in this study. For each AFM image, the average roughness of the surface, its root mean square as well as the peak-valley height were measured and then averaged by using three samples per pH condition.

.

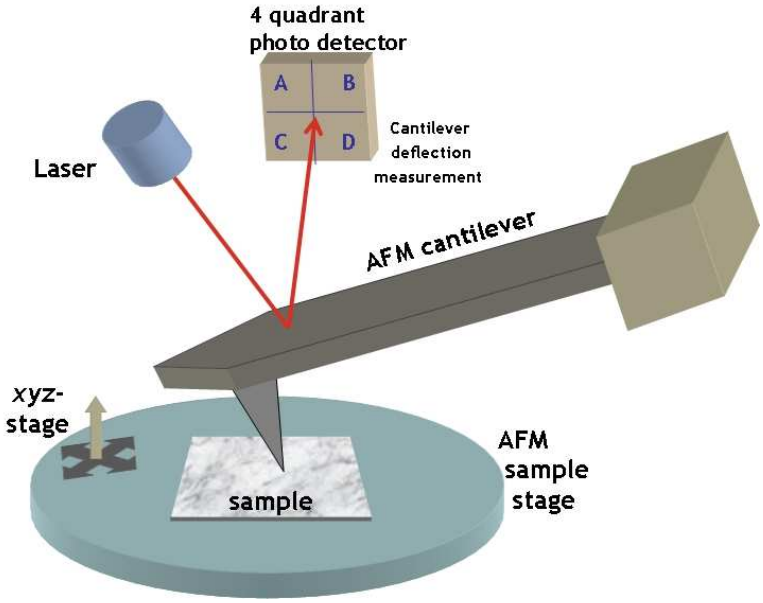

Figure 6: Schematic of AFM principle[72]

IV. Impact of the assembly pH on the BMP-2 release

1. Comparative study up to 25 days

The sandwich ELISA protocol used was specific for BMP-2, allowing for determination of BMP-2 concentration in the release medium for each pH condition and at each time point, eventually resulting in Figure 7. For PEMs prepared at the lowest pH value (pH = 4.0), the amount of BMP-2 released is the greatest and reaches approximately 1.80 ± 0.11 μg/cm² after twenty-four days. As the assembly pH becomes more basic this amount decreases gradually, reaching its minimum release profile for coatings assembled between pH = 6 and pH = 7 with roughly 790 ± 160 ng/cm² of BMP-2 released in the same time span. However, when the deposition pH increased further, the amount of BMP-2 released from the PEM increased, resulting in 1.20 ± 0.085 μg/cm² of cumulative release after 25 days for plates prepared at pH = 8.

Two reasons could explain these differences in release profiles. The first one is that the amount of BMP-2 initially adsorbed on each plate before the PEM formation was not always the same. However, as all plates were anodized and immersed in the same BMP-2 solution by following the exact same protocol, this hypothesis does not seem to hold. The more plausible reason is that the PEM internal structure was sensitive enough to the difference in assembly pH that it adopted different architectures as a result. As a matter of fact, after several weeks of experiment, all samples would have reached an internal pH equal to the one of the surrounding medium, namely 7.4. Therefore, the different behaviors that were observed, especially at the end of the study, have a very low probability of being due to events happening after the PEM formation. Following this reasoning, the various profiles that were obtained were predetermined before the actual release study started. The only variable that could have had such an impact was the PEM deposition pH. The deposition pH-dependent variations in internal organization would be then reflected in the BMP-2 release profiles, as

the molecules would encounter more or fewer obstacles when trying to diffuse from the titanium substrate through the multilayer.

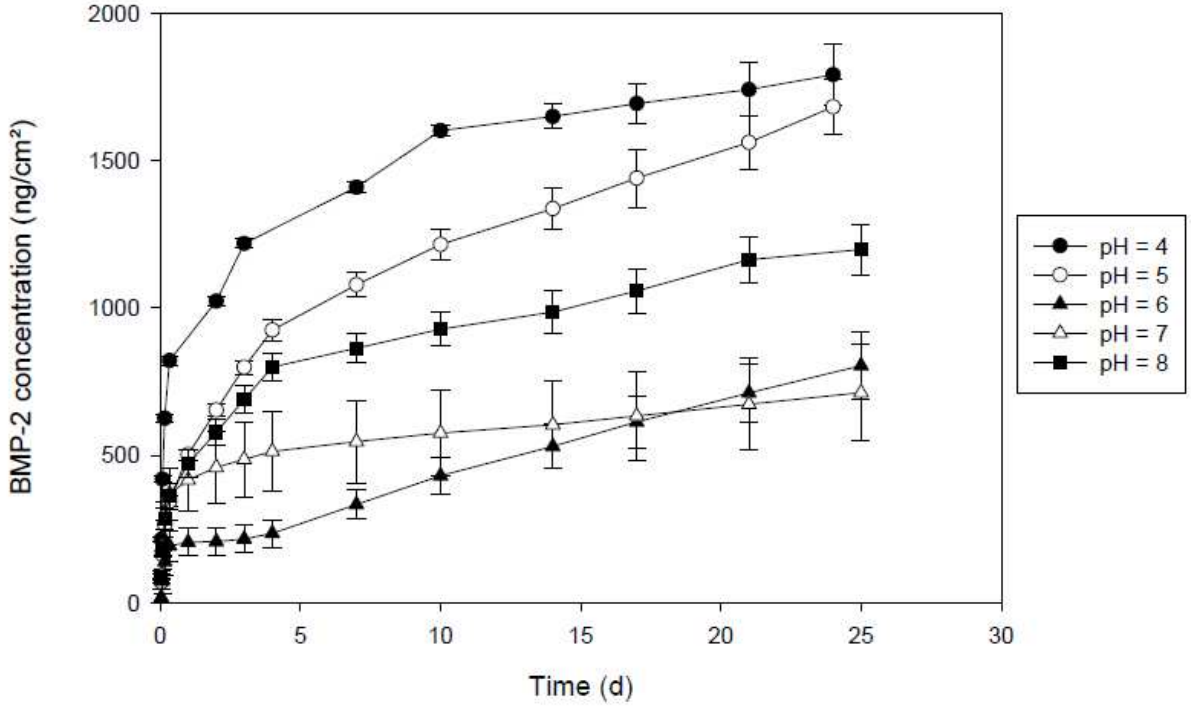

Figure 7: Cumulative released BMP-2 concentration for various assembly pH. Error bars represent standard deviation.

Based on this understanding of BMP-2 release, a smaller amount of BMP-2 released after a certain time span would indicate that the PEM coating is more stable and/or packed more tightly than for other pH conditions. As a matter of fact, Peterson et al. have shown that PMAA has a very low solubility in water, especially in a pH range of 5.7-7.7 [61], which might explain the increased resistance to BMP-2 elution of the studied PEM prepared around pH = 6. Nonetheless, this increased resistance of the coating also has the potential of an extended period of release that could span way longer than 25 days.

On a different note, it is interesting to point out that independently of the assembly pH, all samples presented sustained release for up to 25 days. Knowing that the biological fixation of the implant, that is to say the proliferation of cells aiming to anchor the foreign body into the skeleton, starts 10-14 days after surgery and that the mineralization of these new tissues can take more than

three months,[4] such results are extremely promising for the use of this BMP-2 system as implants coating.

Plotting the BMP-2 concentrations in term of their percentage compared to the initial total amount of BMP-2 adsorbed on titanium plates yielded results leading to identical observations as plates prepared at pH = 6 presented the lowest release percentage (Figure 8). However, it was noted that for all pH conditions, the amount released at the end of the 25 days experiment was consistently above 90%. Following this observation, the initial total amount of BMP-2 adsorbed on the titanium plates should have been around 835 ng/cm², which is the value obtained by the plate prepared at pH = 6, and, moreover, this amount should have been the same for all plates as explained previously. There are thus conflicting results between the measured BMP-2 concentrations displayed in Figure 7 and the corresponding percentages presented in Figure 8.

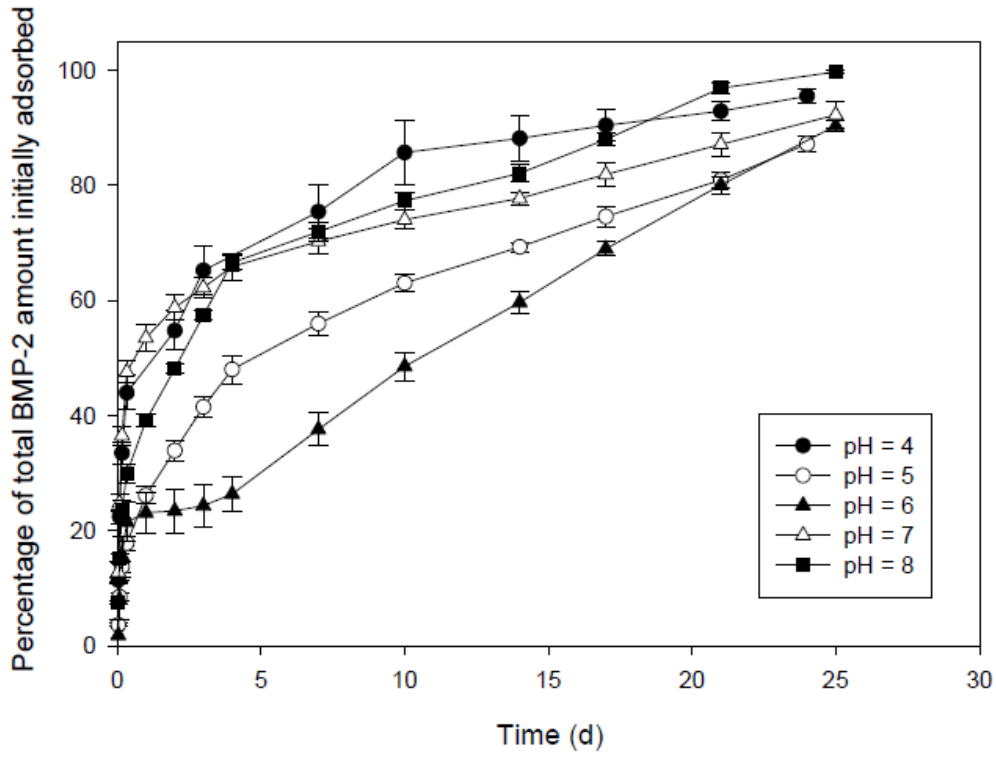

Figure 8: Cumulative percentage of released BMP-2 for various assembly pH. Error bars represent standard deviation. The total amount of BMP-2 released at the end of the experiment was identified to be the total amount of BMP-2 initially adsorbed.

As there would be no reason for different quantities of BMP-2 to be adsorbed while following the same immersion protocol, another explanation was pushed forward, namely, the assumption that the final plate treatment aiming to peel the PEM and the remaining adsorbed BMP-2 did not fully capture all BMP-2 that was left in the system (both on the titanium substrate and within the PEM). In order to confirm this new hypothesis, the release studies taking place at the time were not stopped after 25 days but pursued until a state of BMP-2 depletion could be approached.

2. Complete release profile and kinetics

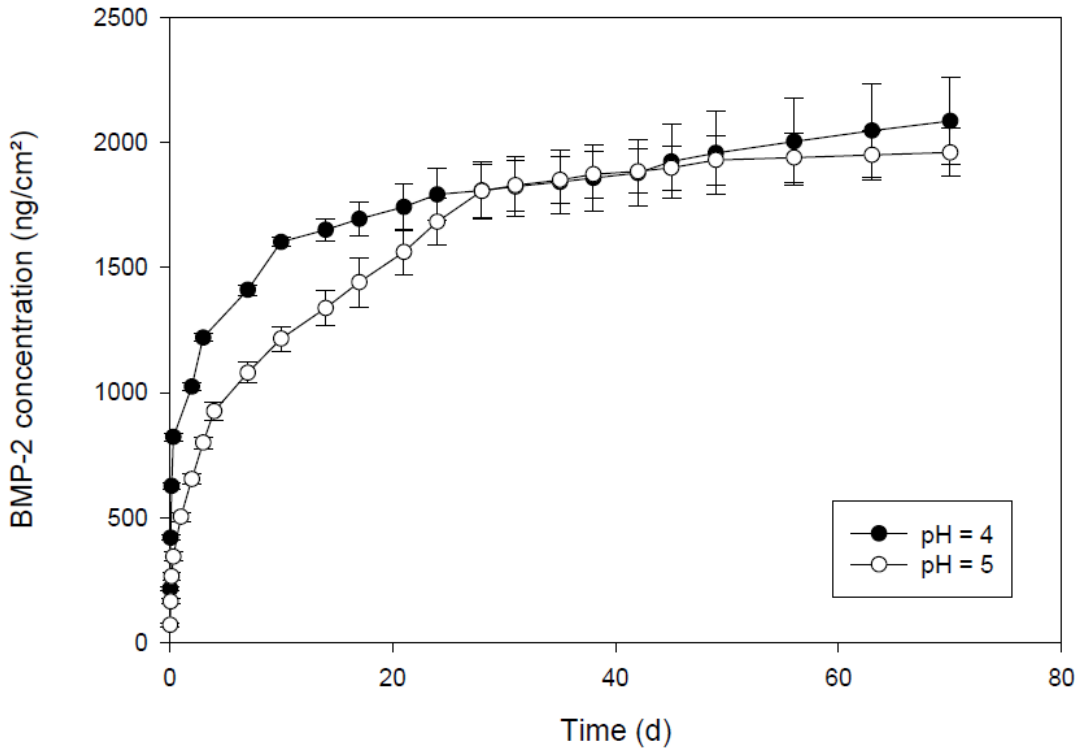

Figure 9: Cumulative released BMP-2 concentrations for coatings assembled at pH=4 and pH=5. Error bars represent standard deviation.

The release studies for samples prepared at pH = 4 and pH = 5 were performed for up to seventy days. At this point, a leveling of the release profile extending to the last few weeks was observed, indicating that almost all BMP-2 had been let out of the PEM (Figure 9). This assumption

was furthermore supported by the similar aspect of the curves representing the BMP-2 concentration percentage (Figure 10) and the nearly identical value of cumulative BMP-2 release attained at the end of both release studies, establishing that the total amount of BMP-2 adsorbed on each plate was around 2.0 ± 0.13 μg/cm² and that the final process aiming to clear the plate of all remaining BMP-2 adsorbed was indeed inefficient. In that regard, the percentages presented in Figure 8 could be considered inaccurate and should be recalculated, either by assuming an average initial amount of BMP-2 adsorbed equal to 2 μg/cm² or, to ensure scientific soundness, by redoing the release studies and monitor the BMP-2 release until its profile indicates an exhaustion of the initial load, as was done in this experiment for pH = 4 and pH = 5.

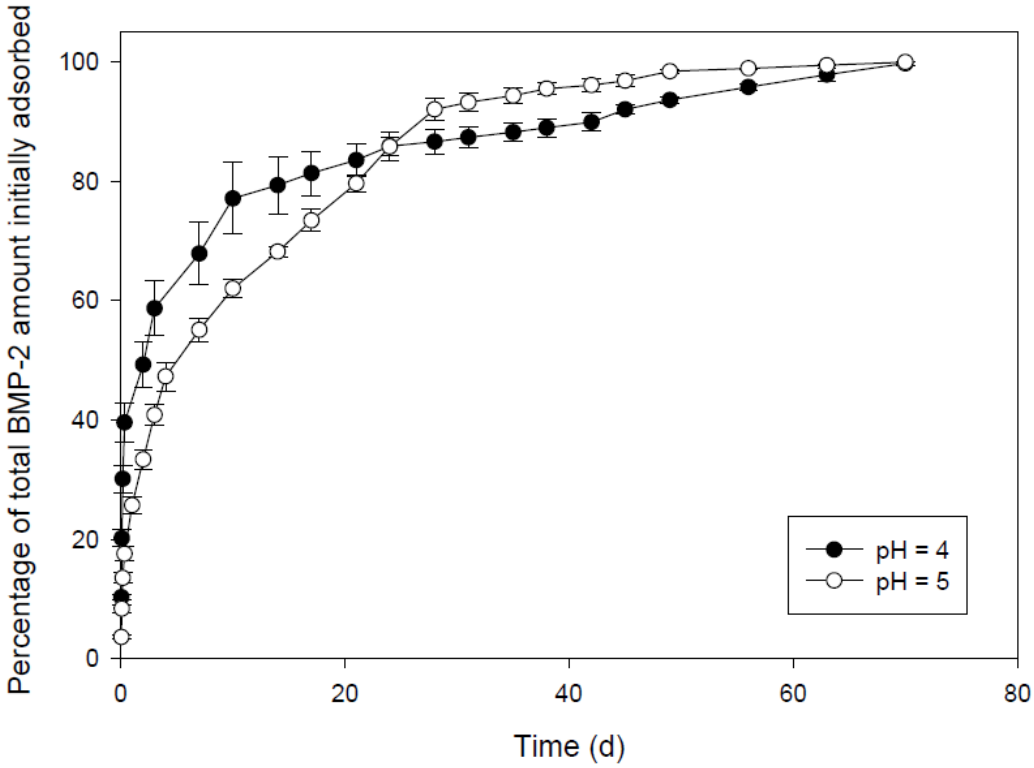

Figure 10: Cumulative percentage of released BMP-2 for coatings assembled at pH=4 and pH=5. Error bars represent standard deviation. The total amount of BMP-2 released at the end of the experiment was identified to be the total amount of BMP-2 initially adsorbed.

Peterson et al. reported similar amounts initially adsorbed for the release of fluorescent-labeled poly-lysine from a PLH/PMAA multilayer.[61] When switching to the release of BMP-2 molecules however, other studies from this group showed that the initial amount of proteins adsorbed on the

substrate ranged between 20 and 100 ng/cm².[44,64] These differences in magnitude order are most probably due to the different protocols followed in these experiments, the main ones being the release temperature (room temperature for Peterson et al., 37 °C in the present report) and the pH of the rinsing water when building up the PEM (unchanged for Peterson et al., pH adjusted in the present report). Additionally, other studies about BMP-2 release indicated that high amount of molecules can indeed be released depending on the PEM formation conditions and on the release conditions. Guillot et al. as well as Crouzier et al. both used a system alternating poly-L-lysine and hyaluronic acid and observed concentrations ranging from 6 to 15 µg/cm² of growth factor being released from the PEM. Crouzier et al. used a porous ceramic as a substrate, whereas Guillot et al. used titanium.[52,53] Similarly, MacDonald et al. reported as much as 10 µg/mm³ of BMP-2 released in vivo from a 14 mg scaffold coated with a poly(β-aminoester)/chondroitin sulfate multilayer.[43] The results displayed in this report are thus plausible and tend to confirm that several complex phenomena oversee the release process. These results also demonstrate the potential of this PEM coating as a long-term delivery system, as its effectiveness could be witnessed for more than two months, which represents two thirds of an implant osseointegration. Complete release profiles at other deposition pH values should thus be investigated in order to confirm these already promising results, especially for coatings assembled at pH = 6, as their great stability could extend the release period even further.

	Transition I/II		**Transition II/III**	
pH	**t (d)**	**BMP-2 concentration (ng/cm²)**	**t (d)**	**BMP-2 concentration (ng/cm²)**
4	0.3535	903.83	10.138	1645.15
5	3.2124	898.74	27.628	1824.92

Table 1: Transition points between the different kinetic regimes of release

A point that has not been yet addressed is the mass transfer processes involved in these release studies. From Figure 7 it could be seen that after a burst of released BMP-2 taking place during the first day, the profiles leveled slightly during the first few days. Then, after roughly four days of immersion, an extremely regular release was witnessed until the end of the twenty-five days period. The curves shown in Figure 9 complete this observation by covering a longer span of time. It appears

from them that the first two regimes observed in Figure 7 can actually be merged as one covering the first days of the study, followed by a very steady release for up to 20-30 days. After that point both curves level off, their slopes coming close to zero, eventually establishing what could be considered as three different zones for the profile of each pH condition. Each one of these regimes was fitted with a linear model ($R^2 \geq 0.91$) and the transition data in between them were reported in Table 1. Interestingly enough, it seemed that these transitions occurred not based on the immersion time but rather on the amount of BMP-2 released. However, due to the small size of the data pool this observation was made on, more extensive research is necessary to explore this behavior further.

The first zone corresponds to a burst release phase, a common phenomenon in drug release profiles in polymeric systems. Although it has been observed for numerous PEMs such as PLH/PMAA, poly(β-aminoester)/hyaluronic acid, and poly(β-aminoester)/poly(acrylic acid),[40,64] the underlying mechanisms are still poorly understood. Parameters that probably influence diffusion include the surface characteristics of the substrate and its interactions with the adsorbed drug, the morphology and porosity of the PEM coating as well as the processing conditions.[73] In the experiments reported here, it is quite possible that the immersion of the samples into the release medium is the main cause of the observed burst release, as the dry PEM coatings would undergo a swelling process as water molecules diffuse between the polymer chains.[45] These chains would thus reorganize their network, breaking and forming new electrostatic bonds until completion of a new stable matrix that would be more loosely bound than before due to its hydration. This increased porosity along with unbalanced electrostatic interactions and easier transport due to the presence of water molecules in the multilayer would greatly promote the diffusion of BMP-2. Moreover, a concentration gradient would be established between the BMP-2 covered titanium substrate and the BMP-2 free medium in which the sample is immersed, which could cause an osmosis process, further increasing the release rate of growth factor.

The second regime presents a fairly linear profile over the time range of one to several weeks. Following the previous assumptions regarding the first regime, this transition can easily be explained by steady-state diffusion that is reached after completion of the PEM swelling and reorganization. This

stage of the release, however, is the most interesting one from a medical point of view, as it would allow a controlled and continuous delivery of growth factor over a long period of time. Moreover, the differences in transition time (Table 1) and in speed of release (Table 2) induced by the assembly pH of the coating indicate that this control could be optimized if the corresponding assembly pH were used, thus resulting in precisely tuned BMP-2 eluting PEMs that would be specifically designed for a given release profile. Such steady profiles for a similar multilayer coating have already been reported by Peterson et al.[64]; however, the considerably longer period of steady release as well as the larger amount of growth factor involved that are reported here further increase the potential of this system.

	Slope		
pH	**Regime I**	**Regime II**	**Regime III**
4	1940.4	75.758	7.7379
5	220.03	37.933	3.6892

Table 2: Slope of the different kinetic regimes of release

The third and last regime, in which the leveling of the release profile can be observed, corresponds most probably to the exhaustion of the BMP-2 reservoir adsorbed on the titanium substrate. As less and less growth factor remains on the plate, the previous steady-state would be thrown out of balance once again as a constant diffusive flux could not be maintained through the multilayer. However, unlike the first regime this transition would not end up in a matrix reorganization, as the electrostatic bonds would be mostly dependent on the polymer chains and the solvent molecules rather than on the remaining BMP-2 molecules. As a result, there would simply be a decreased flux of growth factor. Eventually all BMP-2 would be released, an assumption confirmed by the percentage curves (Figure 10).

Up to this point, only diffusive phenomena have been considered to explain the release of BMP-2 into the surrounding medium. Another common process of drug release that could intervene in this system is the degradation of the PEM, which is to say the disruption in the electrostatic bonds linking the different polyelectrolyte layers together because of the water molecules infusing it. This mechanism leads to a decrease in thickness of the multilayer as the polymer chains are pulled out of it.[10,54] As a matter of fact, Peterson et al. observed that one PLH/PMAA system was substantially

degraded (removed from the substrate) after 25 days of BMP-2 release. They also isolated PMAA in the PBS medium.[61] However, if degradation were the driving factor in growth factor release, very few polymer chains would have been expected remaining on the substrate at the end of the experiment. Therefore, the remaining adsorbed BMP-2 should have been easily removed, and as discussed previously through Figure 7 and Figure 8 this was not the case. This mechanism has thus been considered negligible as compared to diffusion.

3. Research of a global model

Despite the recurrent presence of three different regimes for all assembly pH conditions, the variations in regime transition and speed of growth factor release still could not be predicted. A more general model taking into account the whole release process was needed in order to be able to understand and control the BMP-2 release profiles.

The Higuchi model developed in 1961 is a widely used equation, if not the most used one, aiming to describe the release rate of drugs from a solid matrix. Its basic form can be written as:

$$M_t = A\sqrt{D(2C_0 - C_s)C_s t} \quad (2)$$

Where M_t is the total amount of drug release at time t, A is the surface area releasing the drug, D is the Fickian drug diffusivity within the system, C_0 is the initial drug concentration and C_S is the solubility of the drug in the system. This equation can easily be reduced to a simpler form:

$$M_t = K_1\sqrt{t} \quad or \quad \frac{M_t}{M_\infty} = K_2\sqrt{t} \quad (3)$$

With M_∞ the cumulative amount of drug released at infinite time, which should be equal to the initial amount adsorbed on the sample surface, and K a constant reflecting the design variables of the system.[74] It is obvious that the Higuchi model describes a drug transport dependent on the square root of time, much like the release from a thin polymer film using pure Fickian diffusion for which only the

definition of K would differ. These similar forms are consistent with the fact that the Higuchi model was developed using Fick's first law of diffusion, and can thus be considered as being derived from this model. A direct consequence of this form of time dependence is that both models are only valid for the first 60% of the total drug release.[75] Nonetheless, systems such as PLH/PMAA PEMs or chitosan-based hydrogel have been reported to follow this model.[64,76]

The data obtained during release studies were plotted and fitted to the Higuchi model for all points up to 60% of the total amount released at the end of each experiment, and the resulting model parameters were computed in Table 3. It could be concluded from these results that, besides the PEMs assembled at pH = 5 and, to a lesser extent, at pH = 6 and pH = 8, this model does not properly predict the multilayer behavior regarding growth factor delivery. However, this result could have been expected as one of the major hypotheses supporting the Higuchi model is that the polymer carrier diffusing into the outside medium should not swell or degrade during the diffusion process.[75] As discussed previously, the studied PEM does not conform to this hypothesis. Moreover, proteins such as BMP-2 have complex secondary structures that include functional groups and can therefore interact through hydrogen bonds or electrostatic interactions with the polymer matrix. As a result, their diffusion cannot be described using a Fickian diffusion model or one of its variations as such theories were usually developed to account for the diffusion of small, uncharged molecules.[2]

	Higuchi model		**Power law model**		
pH	**K**	**R^2**	**K**	**R^2**	**n**
4	792.05	0.5791	817.67	0.9212	0.2778
5	424.64	0.9595	457.09	0.9672	0.435
6	138.78	0.8679	174.22	0.8705	0.4303
7	349.36	0.3988	349.91	0.875	0.242
8	435.29	0.8769	430.12	0.9528	0.3497

Table 3: Model parameters for the Higuchi and the power law models

Following this observation, other models were considered such as a zero-order kinetic behavior and the power law model, which can be written as:

$$\frac{M_t}{M_\infty} = K.t^n \quad (4)$$

It can be seen that the Higuchi and Fickian models are obtained when n = 0.5, whereas the zero-order model corresponds to the case where n = 1, which means that the drug release would remain constant over time. This last model has been sometimes found consistent with complete drug release profiles for PEM systems as reported by Berg et al.;[77] however, in most cases a zero-order model was only representative of a later stage in the release process.[40,76] From Figure 7 it can indeed be concluded that this model, if fitting for the constant release observed after one week, cannot be used to account for the complete release behavior. As a result, each BMP-2 profile was fitted to the power law model. The results are shown in Table 3.

Overall, all pH conditions agreed fairly well with a power law, with a coefficient of determination greater than or equal to 0.87 and a power below 0.5. Extending the model to the release studies lasting seventy days confirmed these results for pH = 4 and pH = 5 with coefficients of determination equal to 0.92 and 0.96 and power orders equal to 0.246 and 0.397, respectively. From this analysis, it can be concluded that, if a Fickian or Higuchi diffusion mechanism is indeed involved in this release process, it is not the only one actively participating in the transport of BMP-2 from the substrate to the outside medium. It has notably been reported by Siepmann and Peppas that the increased plasticity of the multilayer caused by the hydration of the polymer matrix can enhance molecule transport through what is referred as a case-II mechanism. These two phenomena, diffusion through the PEM as well as transport induced by a dynamic swelling, should thus be both taken into account in order to devise an accurate model of drug release from PEMs.[75] Moreover, the variations of deposition pH incidentally modifying the multilayer swelling can also impact these mechanisms by increasing or decreasing their relative contribution to the transport phenomenon. Finally, the electrostatic interactions between BMP-2 molecules and the polymer matrix cannot be neglected as such interplay is highly important during the release process.[78]

V. Impact of the assembly pH on the PEM structure and formation mechanism

As conditions during the release study were identical for all samples, the differences observed in amounts of released BMP-2 could only be explained by a deposition pH-dependence of the multilayer coating that would affect its internal structure. Such behavior has been previously reported, while the effects described are sometimes completely opposite for different PEM complexes. Garg et al. observed that increasing the solution pH when building up a PEM of poly(allylamine hydrochloride) (PAH) and PCBS, an anionic polymeric dye, resulted in an overall increase in mass adsorbed as well as an increased thickness of the PEM.[79] However, Notley et al. reported that PAH/poly(acrylic acid) (PAA) systems were thicker when formed at more acidic pH values.[68] Finally, the poly(L-glutamic acid)/poly-L-lysine (PGA/PLL) coating studied by Richert et al. showed an increase in thickness if either highly acidic or highly basic pH were used during its formation, whereas it remained thin between pH = 6 and pH = 8.[80] In order to investigate if and how the assembly pH would indeed impact the BMP-2-$(PMAA/PLH)_5$ system, QCM-D measurements were performed at pH = 6 and pH = 7.

1. The Sauerbrey model

QCM-D is a nanogram sensitive technique that uses acoustic waves generated by a piezoelectric quartz crystal sensor to measure mass. The reference frequency f_0 for these sensors is usually equal to 5 MHz, which corresponds to a crystal thickness of roughly 330 μg.[81] The measured shift in frequency of the acoustic waves can be linked to the mass adsorbed onto the sensor using the Sauerbrey equation which was developed in 1959:

$$\Delta m = -C.\frac{\Delta f}{n} \quad (5)$$

Where m represents the mass, f the frequency, n the overtone number and C the mass sensitivity constant, equal to 17.7 Hz.ng/cm^2 for a 5 MHz crystal and defined as:

$$C = \frac{t_q.\rho_q}{f_0} \quad (6)$$

With t_q the crystal thickness and ρ_q its density.

Despite its simple form, the Sauerbrey equation has been widely used in QCM analysis to investigate adsorption phenomena and surface functionalization such as *in situ* hybridization of DNA, detection of cellular systems, adsorption of proteins and lipids or even model for cell adhesion.[82] The validity of the Sauerbrey equation is dependent on the following three requirements:

1. The adsorbed mass must be small relative to the quartz crystal mass.
2. A rigid film must be formed upon adsorption.
3. The quartz crystal sensor must be homogeneously covered by the adsorbed film.

Many PEMs comply to these conditions and thus their kinetics during the multilayer formation have been extensively researched using the Sauerbrey model.[83–85] This fact can mostly be explained by the very thin films obtained, with thicknesses ranging from a few nanometers to a few hundred nanometers depending on the polyelectrolytes used, the number of bilayers and the assembly conditions.[39,59,86] Kolasinska et al. indicated that the thickness of a five bilayer PSS/PAH system ranged from about 3 to 8 nm.[87] Similarly Köstler et al. reported a thickness of about 17 nm for PDADMAC/PSS PEMs containing five bilayers. As will be discussed in greater detail in section (V.4), the BMP-2-(PMAA/PLH)$_5$ system presented here was deemed compatible with the use of the Sauerbrey theory and investigated through QCM-D in order to determine how the assembly pH would impact the mass and structure of the PEM.

2. PEM adsorption profile and importance of solutions filtration

Initial QCM-D experiments at pH = 6 and pH = 7 yielded surprising results, as the adsorbed mass profiles were entirely different from what was expected based on a review of the literature. Instead of regular step-like increases in mass corresponding to the different layers being adsorbed, features such as irregular peaks and unexpected decreases in mass were observed (Figure 11). These characteristics were even more pronounced for PEMs assembled at pH = 7, where large amounts of mass were adsorbed during deposition and then were immediately washed away from the surface during the rinsing step (Figure 12). Moreover, the repetition of these experiments to confirm the data obtained led to completely different profiles which did not fit the previous results, while still presenting the same kind of discrepancies.

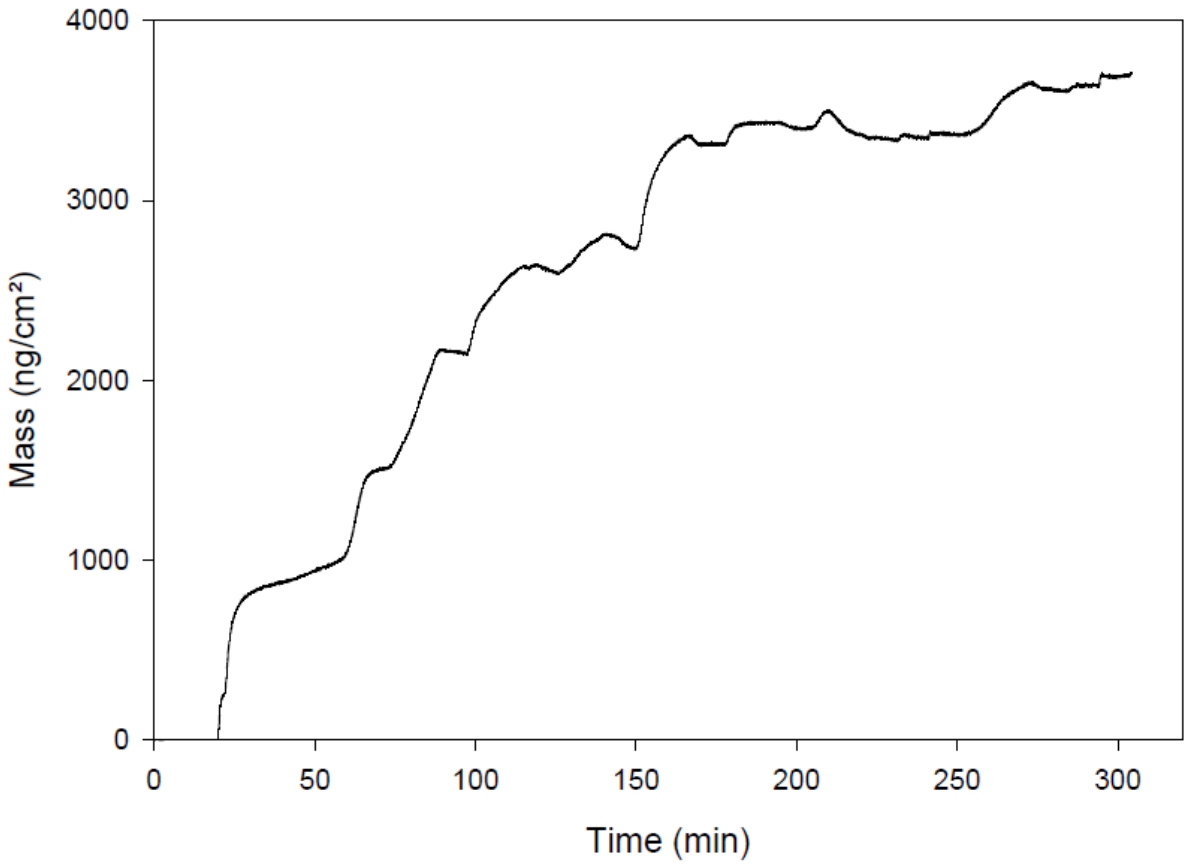

Figure 11: QCM-D curve obtained for solutions and rinsing water adjusted at pH = 6, non filtered. Mass was obtained through analysis of changes in frequency using the Sauerbrey equation.

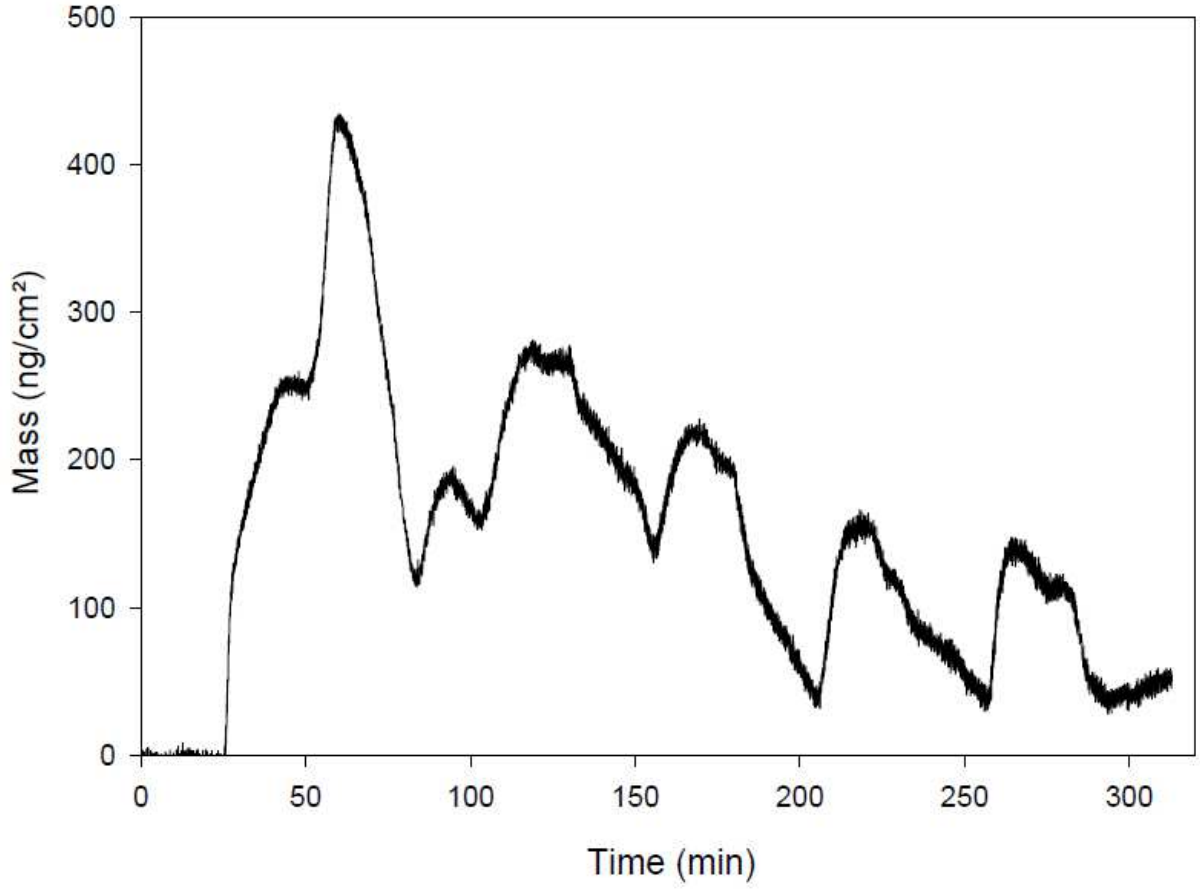

Figure 12: QCM-D curve obtained for solutions and rinsing water adjusted at pH = 7, non filtered. Mass was obtained through analysis of changes in frequency using the Sauerbrey equation.

To explain and remedy to these problems, the highly sensitive conformation of the polymer chains in solution was considered. It has long been known that, because of the charged functional groups attached to the polyelectrolyte backbone, the conformation of these molecules is extremely dependent on parameters such as temperature, solution ionic concentration, pH, and polymer concentration. High ionic concentrations obtained by the addition of salt are known to cause charge screening, which in turn allows the polyelectrolyte chain to adopt a more coiled shape and form thicker layers when adsorbed.[88,89] However, this salt effect was not considered as a possible cause of error during this experiment as the amounts of salt added to the solutions to adjust their pH were negligible (~10^{-6} M, see appendix 3). A similar coil transition was also reported by Glinel et al. for systems including poly(N-isopropylacrylamide) (PNIPAM) and its derivatives.[48] Under 32 °C, PNIPAM chains were highly soluble in water due to strong hydrogen bonding. However, above this

critical temperature the hydrogen bond interactions became disrupted, resulting in a collapse of the chains that adopted a globular conformation. Variations in ionic concentration resulted in shifting that critical temperature, and it was noticed that this transition was entirely reversible. As temperature was maintained constant during the experiment, this parameter was also deemed insignificant for the current system.

Globule-coil transitions can also be obtained through pH variations. Koetz and Kosmella reported that PMAA displayed a compact globule form at acidic pH values, as hydrophobic interactions between the methyl groups formed coiled micro-domains along the polymer chains.[90] Their work also indicated that weak polyelectrolytes were especially subject to these conformational pH-induced changes, which can eventually lead to the formation of aggregates stabilized by surface charges and large enough to result in solution turbidity. This last point was especially interesting, as turbidity had indeed been observed while preparing the PLH solutions used in this experiment. The probable coiled conformation of the polyelectrolyte chains supported the results obtained as the adsorption process would be hindered by the small number of charges available on the aggregates surface. These aggregates would form weak connections with the underlying polymer layer, and thus would be easily washed away during the rinsing step. As a result, it was decided to filter the polyelectrolyte solutions before running them through the QCM-D in order to obtain better adsorption profiles. This procedure proved to be effective, as can be seen in Figure 13 and Figure 14. Each profile presented regular increases in mass as a layer was being adsorbed, followed by a decrease and a leveling representative of the rinsing step, as loosely bound polymer chains would be washed away from the surface.

Finally, a last cause of result discrepancies was considered: the validity of the Sauerbrey equation to correctly account for the mass adsorption process. Several alternative models and corrections to the Sauerbrey model have been proposed for the analysis of PEMs.[91–95] This issue will be more extensively discussed later on in this thesis.

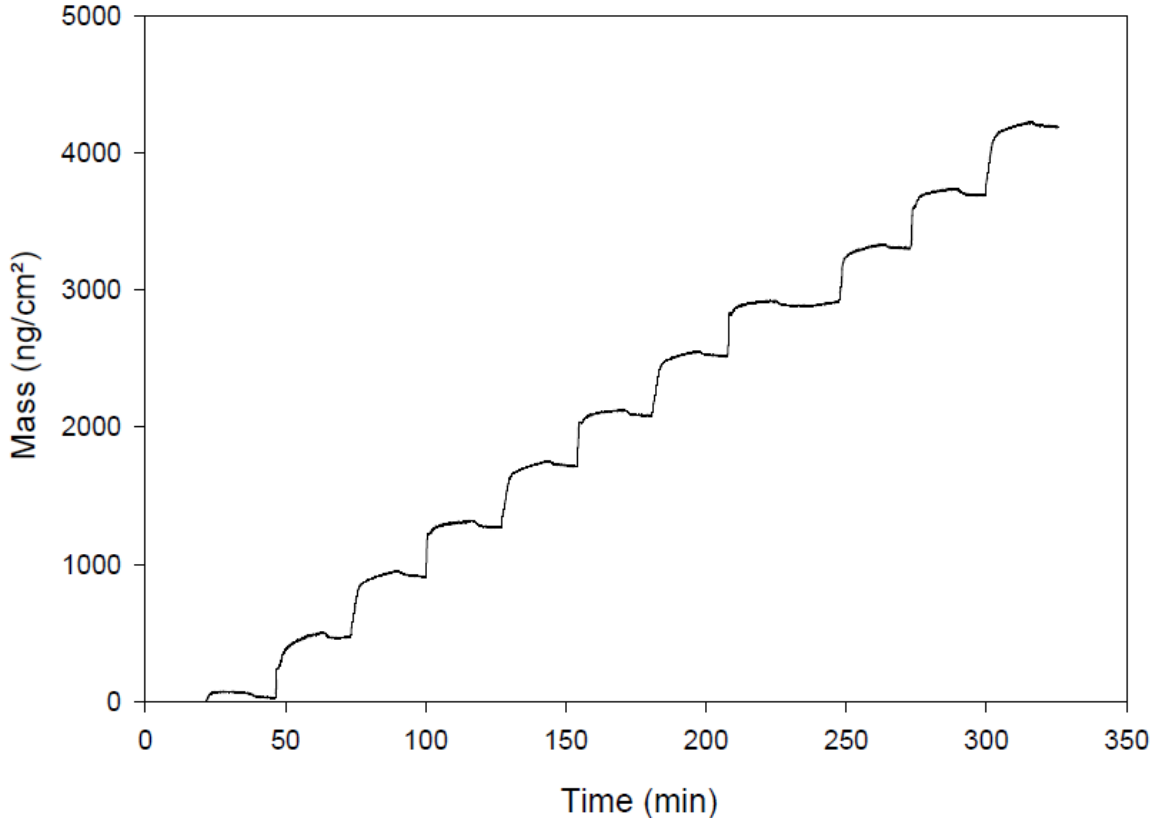

Figure 13: QCM-D curve obtained for solutions and rinsing water adjusted at pH = 6 and filtered. Mass was obtained through analysis of changes in frequency using the Sauerbrey equation.

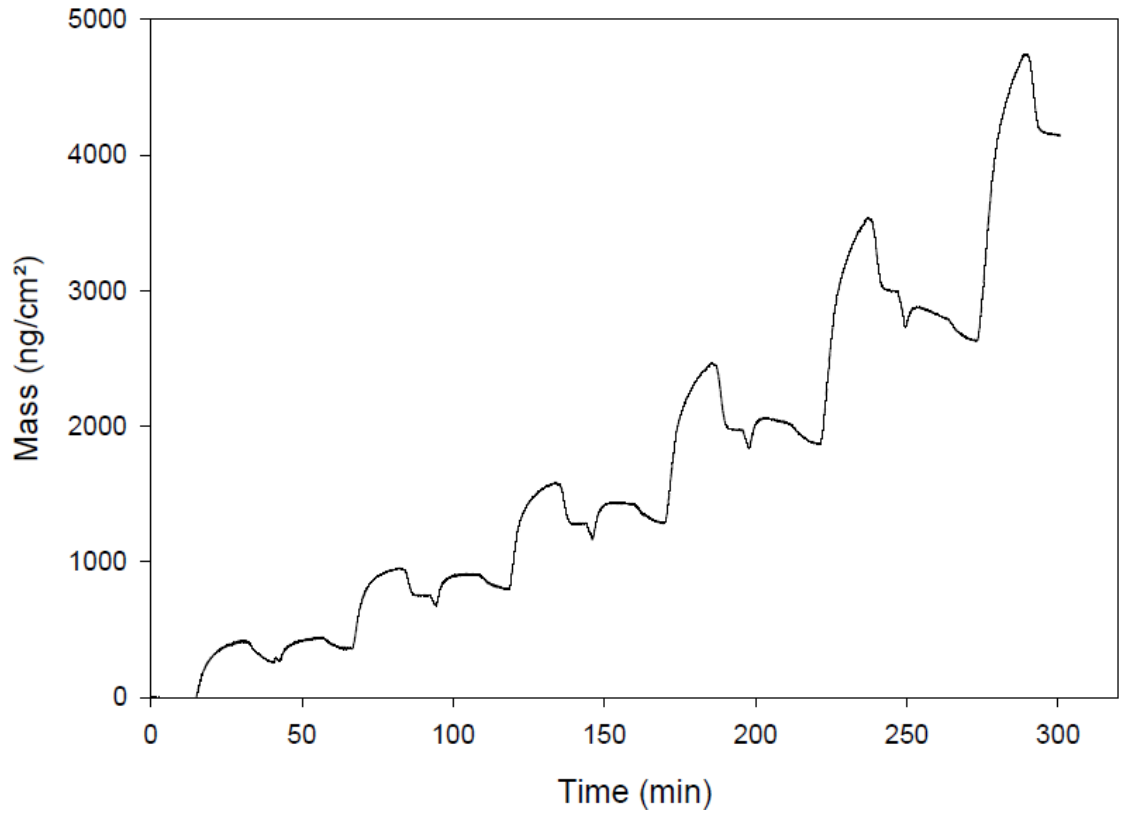

Figure 14: QCM-D curve obtained for solutions and rinsing water adjusted at pH = 7 and filtered. Mass was obtained through analysis of changes in frequency using the Sauerbrey equation.

3. Impact of the assembly pH on the mass adsorbed

Two additional parameters were investigated: the pH of the polymer solutions, either equal to 6 or to 7 for the whole multilayer, and the pH of the rinsing water, either unmodified or adjusted to match the PEM one. For each pH condition, a minimum of four different runs were considered in order to obtain reliable data.

Large variations in mass adsorbed were observed depending on the assembly conditions (Figure 15 to Figure 18). Systems entirely assembled at pH = 6 exhibited an average total mass of 7.6 ± 2.8 μg/cm², whereas a mass of 2.6 ± 1.1 μg/cm² was obtained when using solutions adjusted at pH = 7. Switching from pH-adjusted to regular deionized water also impacted the mass adsorbed, increasing it to 16.4 ± 4.2 μg/cm² for PEMs built at pH = 6 and decreasing it to 1.2 ± 0.68 μg/cm² for the ones formed at pH = 7. Overall, it can be seen that less mass was adsorbed when PEMs were assembled from solutions at pH = 7, and that not adjusting the rinsing water pH had the opposite effects on the adsorbed mass depending on the system pH, as it was increased at pH = 6 and decreased at pH = 7.

Values of PEM mass reported in the literature did not disagree with such a wide range, as they also indicated that this parameter was heavily dependent on both the PEM nature and the assembly conditions. For example, systems made with different polyelectrolytes can show similar mass adsorption for a given number of layers. Notley et al. and Chien et al. reported that PAH/PAA systems consisting of eleven layers had a mass of about 2.5 μg/cm² under certain pH conditions.[68,96] The same estimation of mass was found to be consistent with PEM including several different polythiophenes, as well as chitosan/heparin multilayers, even though they are polymers with extremely different functional groups.[84,97] On the other hand, several studies demonstrated that varying the assembly pH for the same PAH/PAA system resulted in large variations in mass adsorbed, ranging from less than 800 ng/cm² to 8.6 μg/cm² for an eleven-layer PEM.[68,85,96] Moreover, this difference increased as the number of layers increased, as shown by Chien et al. who reported a mass of 5 μg/cm² for a 31-layer

system built at pH = 2, and of 18 μg/cm² for the same system assembled at pH = 6.5, while no significant difference between the two systems could be observed when only eleven layers were adsorbed.[96] Regarding the $(PMAA/PLH)_{5.5}$ PEM presented in this study, Peterson et al. reported a mass of about 11 μg/cm² when it was assembled at pH = 6 and rinsed with unmodified water, which is a value slightly smaller but nonetheless consistent with the results obtained here.[64]

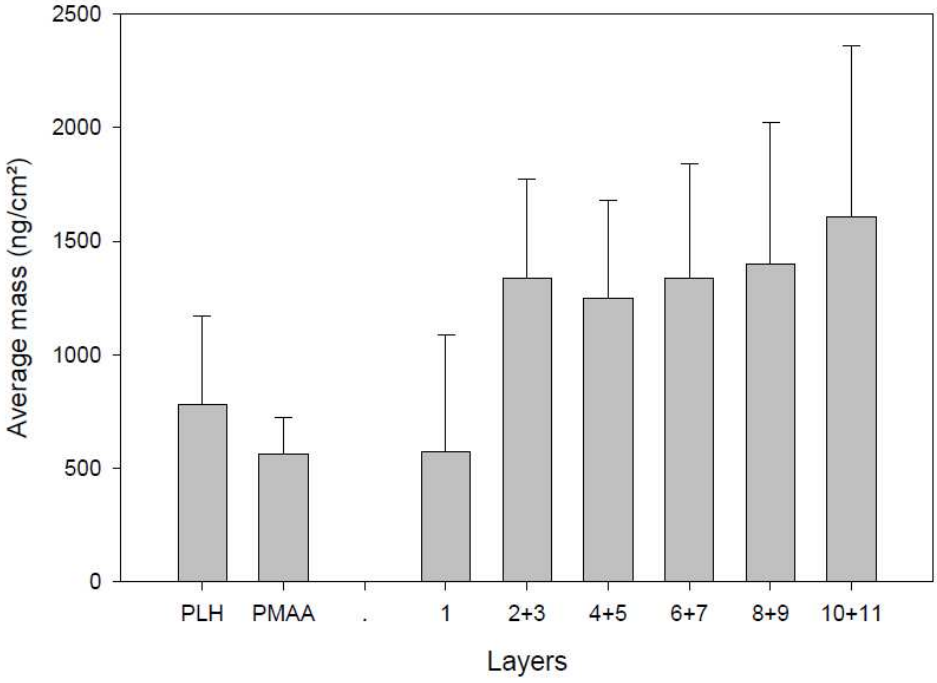

Figure 15: Average mass adsorbed for solutions and rinsing water adjusted at pH =6. Results display the mass adsorbed per layer of a given polyelectrolyte (left) as well as the mass adsorbed per bilayer (right). Error bars represent standard deviation.

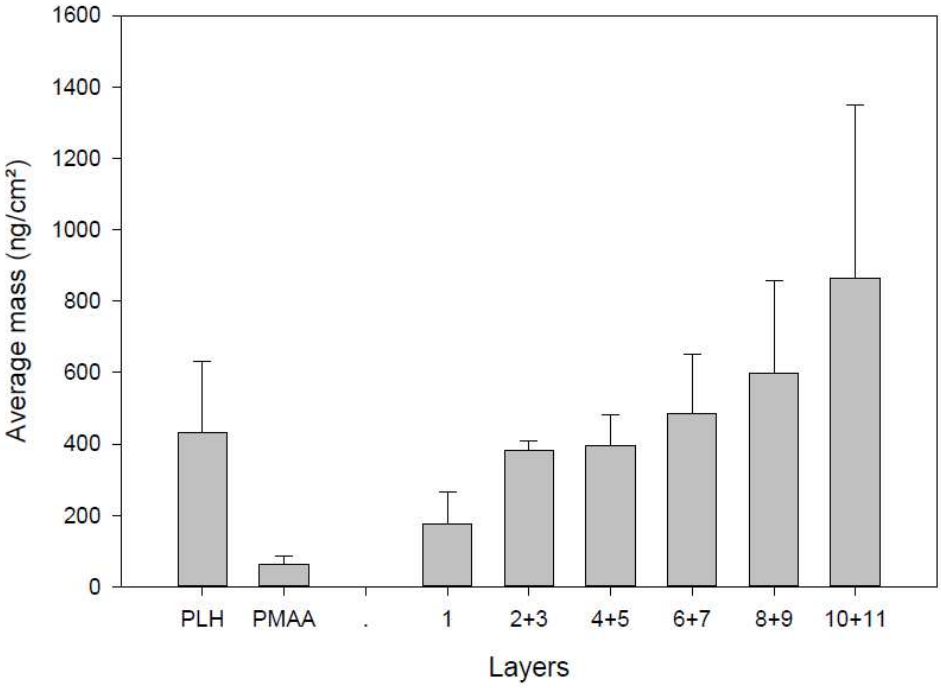

Figure 16: Average mass adsorbed for solutions and rinsing water adjusted at pH = 7. Results display the mass adsorbed per layer of a given polyelectrolyte (left) as well as the mass adsorbed per bilayer (right). Error bars represent standard deviation.

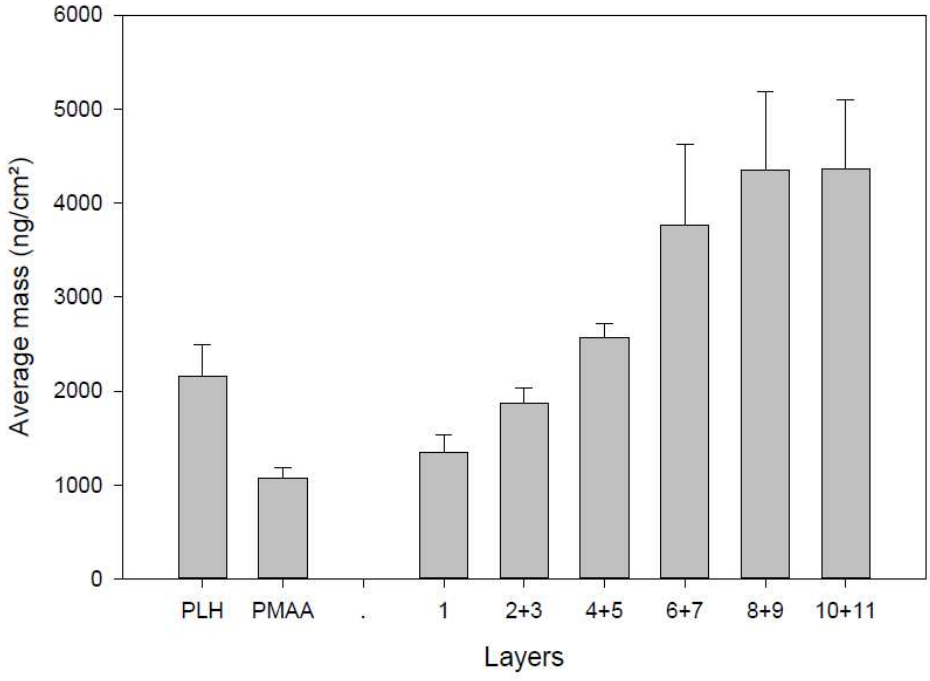

Figure 17: Average mass adsorbed for solutions adjusted at pH = 6 and unmodified rinsing water. Results display the mass adsorbed per layer of a given polyelectrolyte (left) as well as the mass adsorbed per bilayer (right). Error bars represent standard deviation.

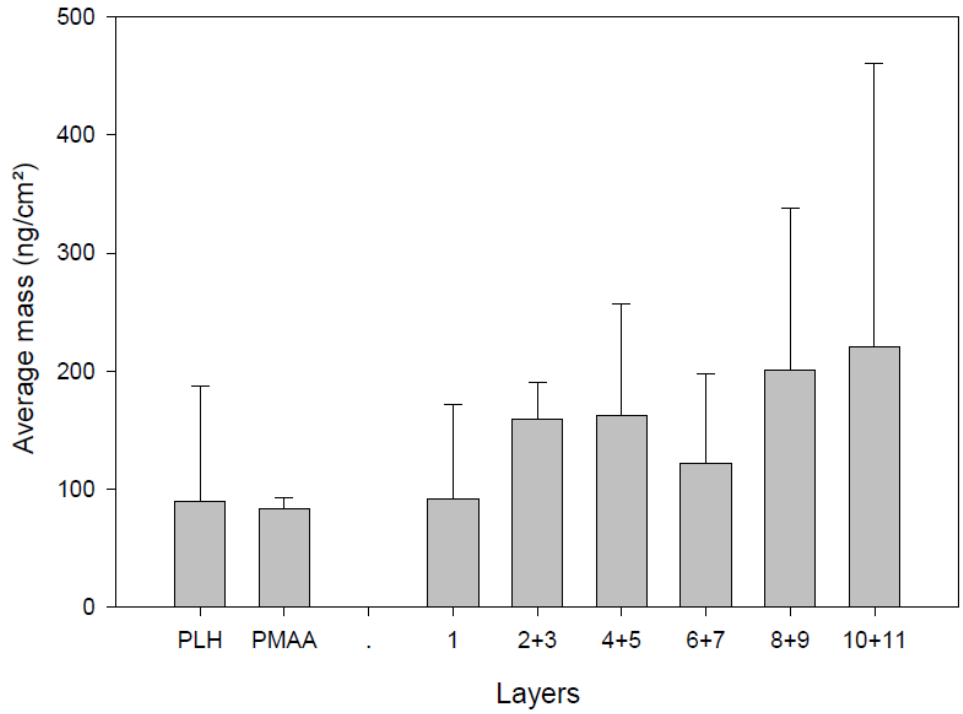

Figure 18: Average mass adsorbed for solutions adjusted at pH = 7 and unmodified rinsing water. Results display the mass adsorbed per layer of a given polyelectrolyte (left) as well as the mass adsorbed per bilayer (right). Error bars represent standard deviation.

It should be noted that, despite performing several runs for each condition, the data obtained in this study still might not be entirely reliable, as they presented extremely large standard deviations - some of these standard deviations were even larger than the actual value they accounted for (Figure 18). In that regard, one should not look at them from a quantitative point of view, but rather from a qualitative point of view in order to identify recurring trends.

One such trend, as was previously mentioned, is the increased amount of mass adsorbed at a more acidic pH value. One explanation for this phenomenon is that the polymer chains present more available charges at pH = 6 due to their overall conformation, which in turn allow more electrostatic bonds to be formed and thus more molecules to be adsorbed in a layer. Moreover, this large number of electrostatic interactions also reinforces the overall stability of the layer, as it will adopt a flatter conformation rather than a loop-and-tail one, making it more difficult to remove molecules from it during the rinsing step. This last point is especially obvious when comparing Figure 13 and Figure 14, as nearly no mass is washed away when building the PEM at pH = 6 whereas a consequent amount of

mass is removed after each adsorption step at pH = 7. These results are consistent with the release study results, as films built at pH = 6 would be more strongly bound than those built at pH = 7, thus offering more resistance to the diffusion of BMP-2.

Another possible explanation to this difference of mass adsorbed, once again due to electrostatic interactions, is the pH-dependent amount of water trapped in each polyelectrolyte layer during its adsorption. Aggarwal et al. reported that this effect could drastically increase the adsorbed mass for a chitosan/heparin PEM that was formed at pH = 4 rather than pH = 9, as the mass fraction accounting for the water trapped in the system jumped from 33% to 71%.[84]

Another observable trend is that more PLH than PMAA was adsorbed per bilayer. Once again, the balance between each polymer ionization level and their resulting conformation can account for this phenomenon. The pKa of PLH ranges from 4 to 5.5 depending on its ionization level, which means that PLH is strongly dissociated at both pH = 6 and pH = 7.[98] On the other hand, PMAA has a pKa of 6.8 and thus presents few charges at pH = 6 and nearly none at pH = 7.[61] Overall, PLH molecules have more possibilities to form electrostatic bonds and adsorb on the PEM surface, which explains why they account for a greater mass.

It can also be seen that the mass adsorbed increased with the number of bilayers. This observation seems to hint that this system does not follow a linear buildup behavior, but rather an exponential one. Elzbieciak et al. as well as Chien et al., among others, reported similar observations for PAH/PAA systems.[85,96] This behavior usually indicates an interpenetration process, which can be described as the polymer chains adsorbing themselves on top of the film and diffusing in the underlying layers at the same time. As this diffusion is enhanced by fewer electrostatic interactions to break, this behavior is especially common for weakly charged polyelectrolytes, which will then adopt a loop-and-tail conformation rather than a flat one when adsorbing on the film surface.[43] This mechanism was consistent with the low ionization degree of PMAA in this experiment. Moreover, it could be seen from Figure 15 and Figure 16 that the exponential growth was more pronounced for PEMs built at pH = 7, which corresponded to a nearly neutral PMAA and further supported this

theory. Films formed at pH = 6 were then probably thinner than those assembled at pH = 7, but also more compact and presenting a higher link density, which in turn would explain why a slower BMP-2 release was obtained from them. The related viscoelastic data (Table 4), which are discussed later on in this thesis, supported this hypothesis, as films assembled at pH = 6 were overall in greater agreement with the Sauerbrey model than those formed at pH = 7.

As was previously said, using unmodified deionized water instead of pH-adjusted water during each rinsing step yielded unclear results as it increased the total mass adsorbed at pH = 6 from 7.6 ± 2.8 μg/cm² to 16.4 ± 4.2 μg/cm², and decreased it at pH = 7 from 2.6 ± 1.2 μg/cm² to 1.2 ± 0.68 μg/cm². Regardless, it is clear that the pH of the rinsing water indeed did matter and impacted the overall multilayer structure during its formation. This processing parameter should be taken into account when designing a PEM coating. The opposite behaviors observed at different pH values were most likely due to the interactions between water molecules and polymer chains. The balance between hydrogen and electrostatic bonds during the rinsing step would be altered when compared to multilayers formed using pH-adjusted water. Moreover, PMAA would be especially sensitive to such changes because this range of pH is very close to its pKa, making PMAA susceptible to switching conformations upon the slightest stimulus and thus impacting the mass adsorbed. To better understand this phenomenon, further studies centered around the rinsing process are necessary.

4. Discussion on possible sources of error

The significant variations of adsorbed mass observed within each pH-condition and the large resulting standard deviations might find their source in several factors. One possible cause of error includes the accuracy of the QCM-D system as well as its artifacts. Castro et al. investigated the impact of an inhomogeneous mass distribution on the sensor surface. They reported that a punctual loading on the quartz crystal surface could lead to positive shifts in resonance frequency, which would then be translated as negative mass shifts when using the Sauerbrey model.[99] These results make

sense, as one of the assumptions of the Sauerbrey model is that the sensor is homogeneously covered. It might also explain some of the discrepancies observed in the present study, as it could sometimes be observed upon dismantling and cleaning the QCM-D setup that the sensors were not entirely covered by the PEM. Another similar source of error includes the fact that, despite extensive cleaning of both the sensors and the entire QCM-D device, some contaminants might have remained in the apparatus between each experiment.

Another criterion to take into account when considering the accuracy of the results is the variations observed in response to specific properties of the coating. It has been shown by Nirschl et al. that when comparing the frequency response of QCM-D and film bulk acoustic resonators (FBAR) during the formation of the same PEM, different thickness values were obtained.[100] Their work suggested that these frequency shifts were mainly due to the penetration depth and the viscoelasticity of the multilayer, which are known to be frequency dependent properties. PEMs demonstrating a significant viscoelastic behavior have especially been known to diverge from the behavior predicted by the Sauerbrey equation.[91,101]

Another assumption of the Sauerbrey model is that the material being measured is a thin rigid film. While many films studied in air can comply with this requirement, coatings assembled in a liquid medium must be considered more carefully as they are hydrated and thus softer, causing part of the resonating energy to dissipate as part of a damping effect.[66,92] Kanazawa and Gordon overcome part of these restrictions by adapting the Sauerbrey equation to purely elastic films formed in liquid media.[93] Similarly, White and Schrag tried to predict the response of a QCM quartz crystal when a viscoelastic layer would be formed on the sensor while being in a viscoelastic surrounding medium.[94] However, the most famous model accounting for both viscous and elastic properties of a soft adsorbed layer is the Kelvin-Voigt model.

The Kelvin-Voigt model, also simply called the Voigt model, consists of a spring and a dash-pot in parallel (Figure 19). The spring accounts for the elastic behavior of the polymer layer and the dash-pot represents the viscous part of the behavior.

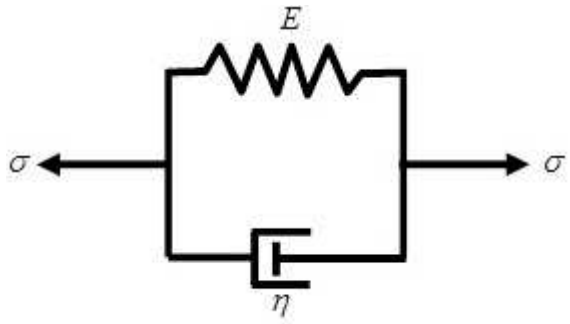

Figure 19: Scheme of the Kelvin-Voigt model

This model assumes that both elements experience the same strain ε, and that the overall stress σ is equal to the sum of both stress contributions. Defining the spring stress and the dash-pot stress respectively as:

$$\sigma_{spring} = E.\varepsilon \quad and \quad \sigma_{dash-pot} = \eta.\frac{d\varepsilon(t)}{dt} \tag{7}$$

With E the spring stiffness and η the viscosity of the material, σ can eventually be written as:

$$\sigma = \sigma_{spring} + \sigma_{dash-pot} = E.\varepsilon + \eta.\frac{d\varepsilon(t)}{dt} \tag{8}$$

Which is the general equation for the Kelvin-Voigt model. It can be seen from Equation 8 that if a stress σ is applied to the system, the spring will want to stretch but will be held back by the dash-pot, which requires a longer time to react to the stimulus. Similarly, if the stress is removed, the spring will want to contract but will be slowed by the dash-pot, thus accounting for dampening effects.[102]

This model has been widely used in PEM and proteins studies to account for behaviors diverging from the Sauerbrey theory.[79,91,103] Moreover, work has been performed in order to expand the Kelvin-Voigt model to more accurately represent the formation of PEMs. One example is the model proposed by Voinova et al. for a two-layer viscoelastic polymer coating, whereas the basic model considers only a single layer. However, as the Sauerbrey model is more simple and easy to use, it is still preferred to the Kelvin-Voigt model if it can be applied. The limit of its validity is usually defined as the ratio of the dissipation shift between the different overtones ΔD over their frequency shift Δf. The smaller this value is, the stiffer the film will be; however values as high as 0.4 have been

deemed acceptable for PEMs by the QCM-D provider. As this ratio increases, the need to switch from the Sauerbrey model to a viscoelastic one such as the Kelvin-Voigt model becomes more and more relevant.

pH	Rinsing water	$\Delta D/\Delta f$ (10^6 Hz^{-1})	Standard deviation
6	pH-adjusted	0.49463	0.45732
	Unmodified	0.19200	0.25204
7	pH-adjusted	0.46095	0.26063
	Unmodified	2.78061	0.28579

Table 4: Limit ratio for the validity of the Sauerbrey model

The results obtained for this ratio were summarized in Table 4. It could be seen from it that for both conditions involving pH-adjusted water, the ratio was slightly above the validity limit of the Sauerbrey theory. Therefore the use of a viscoelastic model did not seem to be necessary, especially since it was demonstrated that the Sauerbrey model could still be applied to non-rigid films if those were thin enough.[92] Similarly, PEMs assembled at pH = 6 with unmodified rinsing water exhibited a $\Delta D/\Delta f$ value in agreement with the Sauerbrey theory, thus confirming the formation of a thin rigid film under those conditions. As a matter of fact, only the films assembled at pH = 7 with unmodified rinsing water proved to require a different model in order to account for viscoelastic effects. These data tend to confirm previous results hinting at a compact, strongly adsorbed multilayer with chains adopting a flat conformation when adsorbing at pH = 6, and a softer, weakly adsorbed one when adsorbed at pH = 7, with layers made of loops and tails more prone to trapping water molecules and thus adopting a more viscoelastic behavior.

VI. Impact of the assembly pH on the surface roughness

1. Contact angle analysis

In order to determine if the pH used during the PEM formation affected the chemical composition, and thus the surface energy of the resulting coating, static contact angle measurements were performed. The approach proposed by Owens and Wendt[69] was used to calculate the components of the surface tensions of the PEM surfaces.

a. The Owens-Wendt method

As with most theories aiming to identify the surface free energy of a solid, the one developed by Owens and Wendt stems from the Young's equation, which correlates the contact angle, formed by a liquid/vapor interface meeting with a solid surface, with the different interfacial energies involved. It is written as:

$$\gamma_S = \gamma_{SL} + \gamma_L . \cos(\theta) \quad (9)$$

γ_S is the surface free energy of a solid (solid/vapor interface), γ_L is the surface free energy of a measuring liquid (liquid/vapor interface), γ_{SL} is the surface free energy at the solid/liquid interface and θ is the measured contact angle (Figure 20).

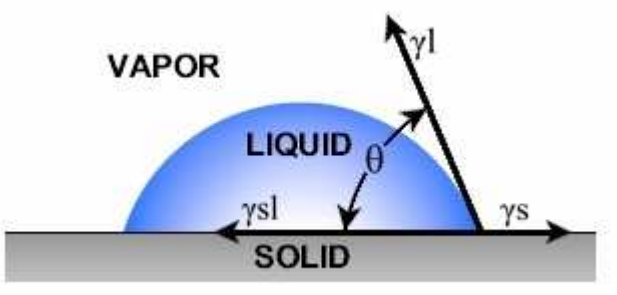

Figure 20: Diagram of contact angle parameters[104]

Another form of this equation is the Young-Dupré equation, which introduce the notion of work of adhesion W_a:

$$W_a = \gamma_S + \gamma_L - \gamma_{SL} = \gamma_L.(1 + \cos(\theta)) \quad (10)$$

Owens and Wendt assumed that both γ_L and γ_S could be divided into a polar part γ^p and a dispersive part γ^d as follows:

$$\gamma_L = \gamma_L^d + \gamma_L^p \quad and \quad \gamma_S = \gamma_S^d + \gamma_S^p \quad (11)$$

Furthermore, they expressed the work of adhesion previously described by using the geometric mean of these surface energy components, leading to:

$$W_a = 2\sqrt{\gamma_L^d.\gamma_S^d} + 2\sqrt{\gamma_L^p.\gamma_S^p} \quad (12)$$

Eventually, the core equation of the Owens-Wendt theory was obtained:

$$\frac{\gamma_L.(1 + \cos(\theta))}{2} = \sqrt{\gamma_L^d.\gamma_S^d} + \sqrt{\gamma_L^p.\gamma_S^p} \quad (13)$$

As the polar and dispersive contributions of numerous liquid have been extensively measured and are easily available in chemistry handbooks, the two remaining unknowns are γ_S^p and γ_S^d, which means one needs to use two different liquids to measure contact angles on a surface while relying on this method. It is recommended to use a liquid with a dominant polar contribution on one hand, as well as one with a dominant dispersive contribution on the other hand in order to minimize the possible error in the determination of the components γ_L^p and γ_L^d. Possible valid associations include water and α-bromo-naphtalene, water and formamide, or even glycerol and diiodomethane. [105]

b. Measurements and results

In order to obtain more accurate results, four different liquids instead of merely two were used to measure contact angles on each sample: water, glycerol, formamide and diiodomethane. Equation 13 was transformed as follow in order to use a linear regression to determine γ_S^p and γ_S^d:

$$\frac{\gamma_L.(1+\cos(\theta))}{2\sqrt{\gamma_L^d}} = \sqrt{\gamma_S^p}.\sqrt{\frac{\gamma_L^p}{\gamma_L^d}} + \sqrt{\gamma_S^d} \qquad (14)$$

The polar and dispersive parts of the sample surface free energy can then be easily determined as the squared value of the slope and the squared value of the intercept, respectively.

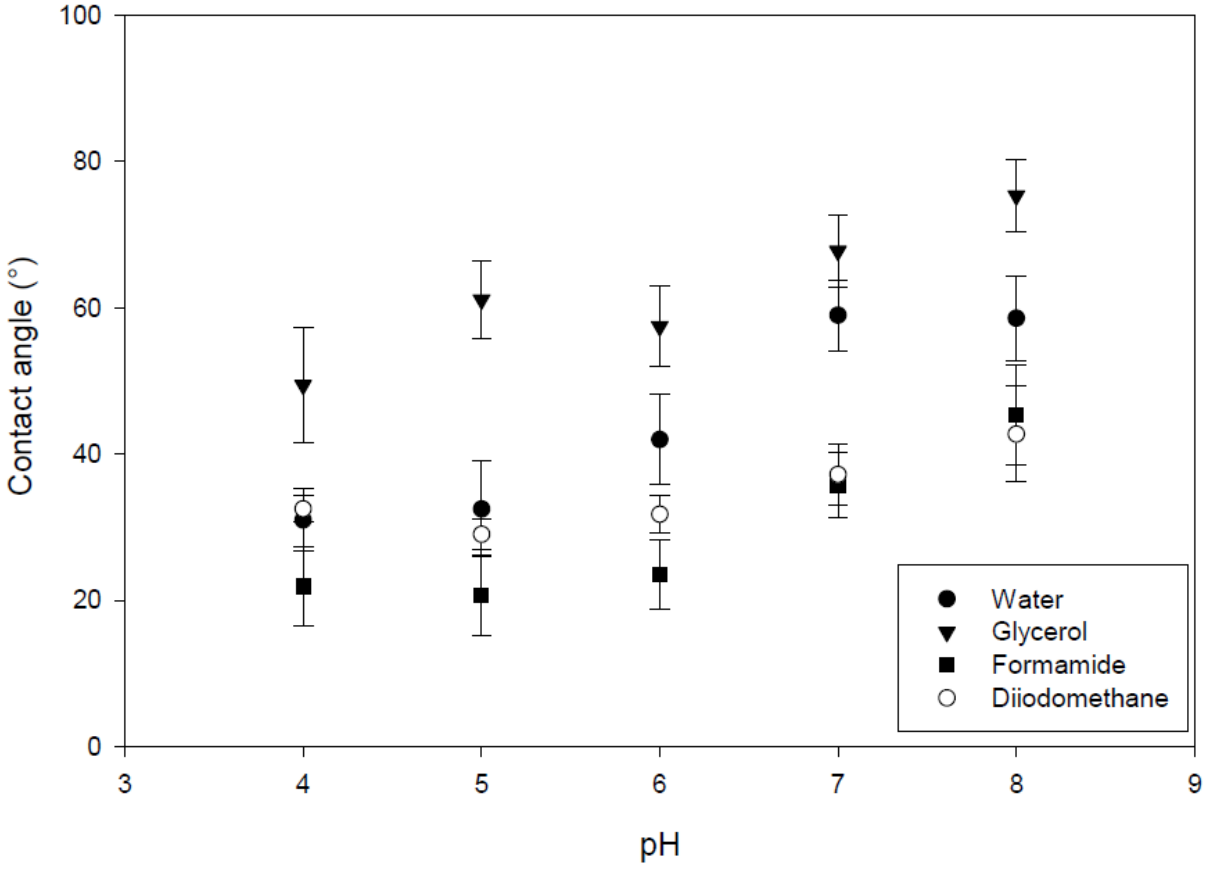

Figure 21: Measured static contact angle of different liquids as a function of pH

For all liquids, a defined trend was observed as the contact angle value increased on plates prepared at a higher pH (Figure 21). This trend was especially visible for pH ranging in between 6.0 and 8.0, suggesting that the coating hydrophobicity was enhanced by using more basic solutions during the PEM buildup. This observation was later confirmed as it appeared that the surface free energy of the coated sample decreased as the PEM formation pH increased (Figure 22).

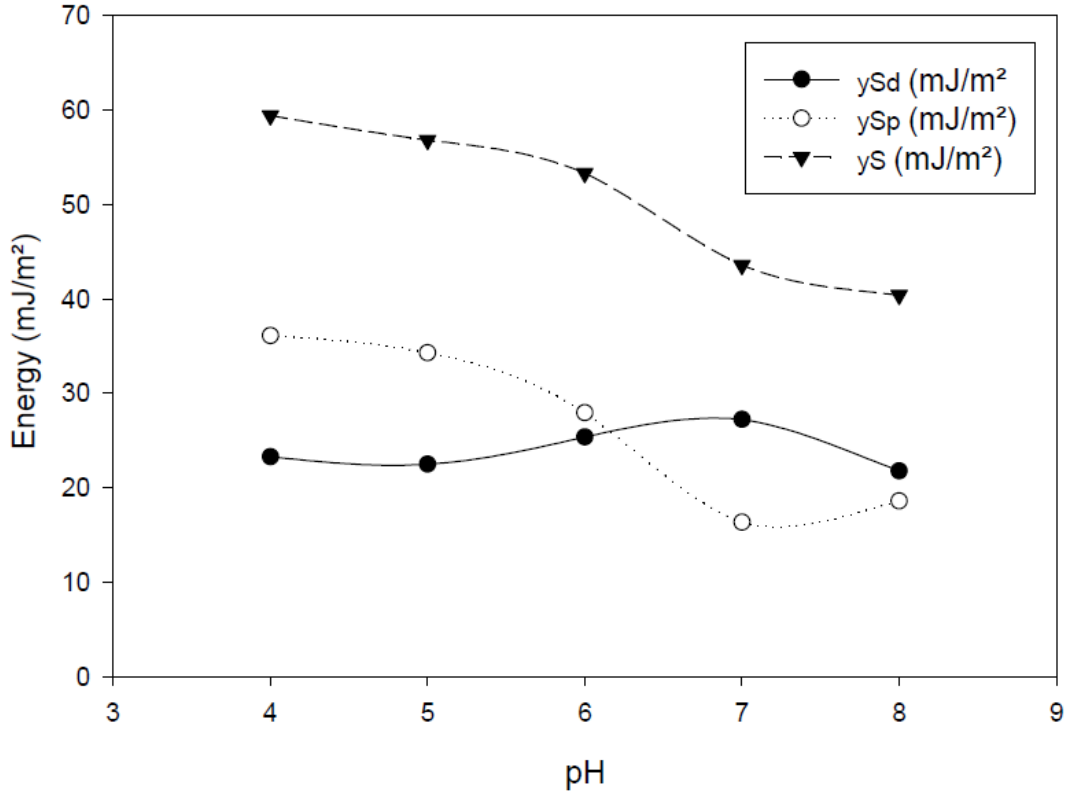

Figure 22: Surface free energy of BMP2-(PMAA/PLH)$_5$ coatings as a function of pH

The polar contribution to the surface energy was dominant for PEM built at more acidic pH and decreased as the basicity of the coating solutions increased, whereas the dispersive component increased slightly when moving from acidic formation pH to basic ones. At these high pH values, this dispersive component became the dominant contribution to the global surface energy. The transition from polar to dispersive dominated regime occurred around pH = 6, for which the polar and dispersive energies presented nearly identical values.

This result was somewhat unexpected, as the final layer deposited for all samples was PLH and thus should have presented the same surface free energy. However, this behavior can be explained by the combined effects of several electrostatic phenomena. The main one is the pH dependency of the charges present on polyelectrolyte chains. As the pH increases, polyanionic chains will see their charge increase, whereas polycationic chains will lose charges, especially if they are weak polyelectrolytes as it is the case in this study.[88] As the final layer of our system consists of positively charged PLH, this means that the charge density on the PEM surface will decrease when prepared at

basic pH and thus will become more and more hydrophobic, eventually leading to the observed experimental results.

Another significant electrostatic effect to take into account is layer interpenetration. It has been shown that the mutual interactions between polyanions and polycations in a PEM could drastically change their pK_a and therefore have a great impact on the multilayer assembly and stability,[59,106] leading to the diffusion of charged chains into an oppositely charged layer. Due to this interpenetration and the generally very small thickness of these systems, the influence of buried layers may still be observed at the PEM surface and impact contact angle measurements. In particular, the work of Köstler, Delgado and Ribitsch has shown that the wetting of these surfaces might lead to a decrease in the upper layer entanglement, thus leading surface properties to resemble the ones of the final layer material.[107] Following this reasoning, it could be expected that all surfaces would behave as PLH, which is the final layer of the PEM. However, the deposition pH-dependent differences in the PEM internal structure also influence the layer entanglement. As a result, various level of loosening upon wetting could be observed for each assembly pH condition. Such entanglement behaviors, influence of lower layers and differences in PEM internal structure could further explain the increased hydrophobicity observed in this study.

Finally, it is interesting to note that at pH = 8 this system presents a surface free energy of 40.42 mJ/m² with a polar and dispersive contributions of 18.62 mJ/m² and 21.8 mJ/m². These values are very close to reported values for the solid surface energy of PMAA (total : 41 mJ/m² , polar : 10.3 mJ/m², dispersive : 29.7 mJ/m²).[108] These results seem to hint to the system surface being chemically close to that of solid PMAA, which is curious because PLH was the last layer deposited. Therefore, the surface free energy should have been closer to that of PLH rather than PMAA. This divergence from expected results can be explained as a result of the delicate balance between the charge density of both polymers when high pH values are reached. As said previously, in this situation PLH chains will become less and less charged, thus leading to a more hydrophobic surface, whereas the PMAA chains will gain more and more charges. Due to layer entanglement, the electrostatic influence of the lower

PMAA layer on the PEM surface energy will therefore become dominant as the PLH layer influence will decrease, eventually reaching values extremely close to that of pure PMAA.

2. AFM analysis

The surface roughness of PEMs designed as possible implant coatings is of utmost importance as it is a key parameter to obtaining good physiological integration of the implant. Numerous studies have shown that several cell responses are dependent on surface topography. In some cases cell proliferation, such as pre-osteoblasts and fibroblasts, was enhanced by flatter PEM surfaces whereas differentiation of those cells was promoted by rougher PEM surfaces.[64,83,109] It has also been reported that parameters influencing PEM roughness include the number of layers, the nature of the polyelectrolyte deposited as a last layer, the assembly temperature, and even the assembly pH.[6,110,111] All of these variables make each PEM system behave in its own unique way when considering the state of its surface, which is why the following AFM study was deemed necessary.

When considering the resulting images, it appears that the differences between all samples are negligible (Figure 23). Independently of their assembly pH, they all present a fairly flat topography with a few blobs as well as irregularities probably due to locally coiled polymer chains or inherent substrate defects. This observation is reinforced by the average roughness and the peak-valley height values of each sample (Figure 24, Figure 25). Indeed, no specific trend linked to the pH variations is visible. This is somewhat surprising, as the work of Gong as well as Niepel et al. clearly indicated that the assembly pH had an impact on the PEM morphology and/or roughness.[110,111] However, the PEM structures they considered differ from the one reported in this study in that an identical initial layer for all pH conditions was not adsorbed before building up their PEM on top of the substrate.

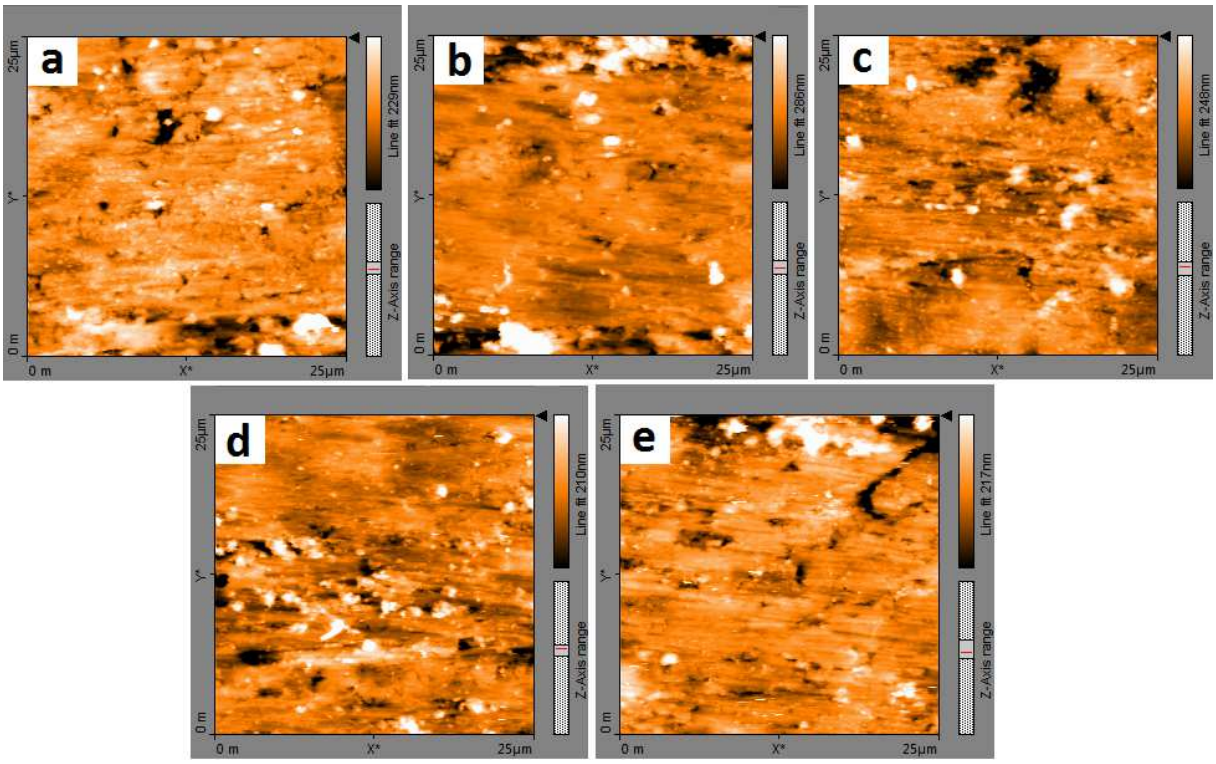

Figure 23: AFM images (contact mode) of BMP-2-$(PMAA/PLH)_5$ multilayers prepared at a) pH=4, b) pH=5, c) pH=6, d) pH=7, e) pH=8. Specified feature size and feature height were 5 µm and 100 nm respectively.

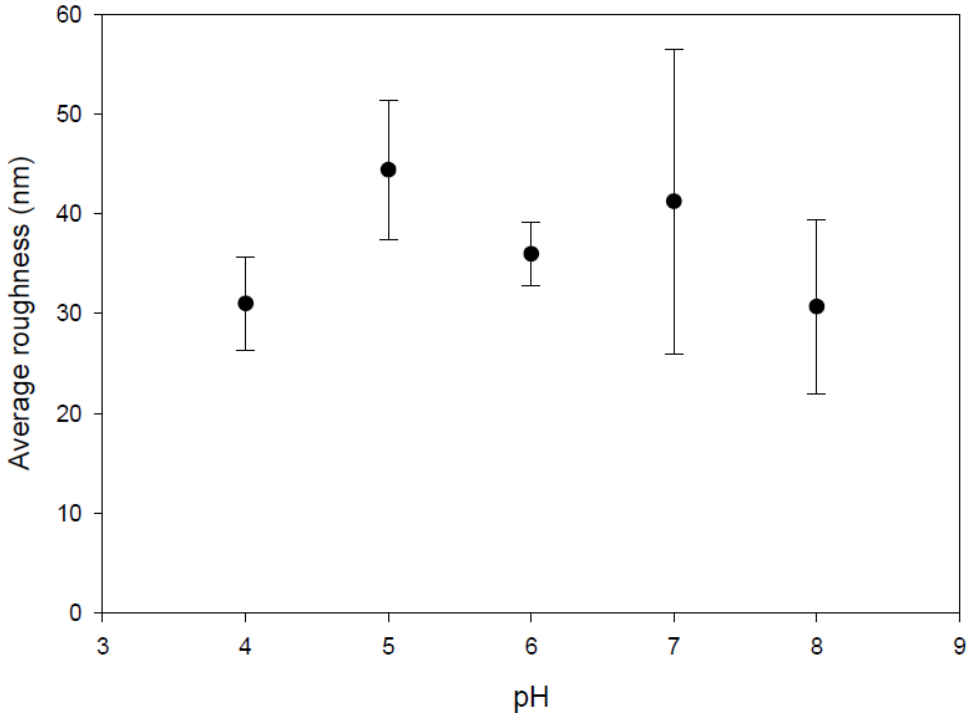

Figure 24: Average roughness of BMP2-$(PMAA/PLH)_5$ multilayers as a function of pH

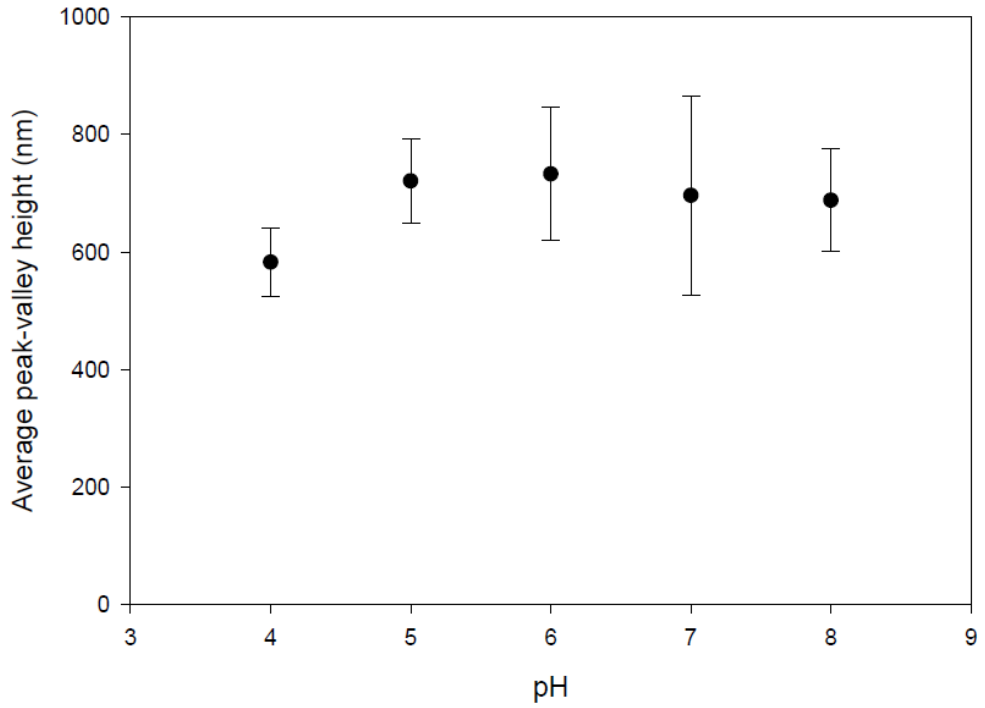

Figure 25: Average peak-valley height of BMP2-(PMAA/PLH)$_5$ multilayers as a function of pH

Kolasinska et al. reported that the deposition of an initial layer of polyethyleneimine (PEI) could deeply impact the whole PEM structure.[87] These effects included a more uniform growth of the film visible even for the first few layers, whereas formation in absence of this first PEI layer resulted in the presence of voids in the adsorbed layers. The most interesting result, however, was the fact that the influence of the PEI layer could be witnessed even at the PEM surface. As a matter of fact, films including this anchoring layer presented a smoother surface as well as different wettability properties as compared to films without an initial layer of PEI, proving that the PEI influence extended as far as fourteen polyelectrolyte layers. Similarly, Peterson et al. reported that when including an initial layer of BMP-2 to their PEM structure, the resulting surface roughness was increased compared to films devoid of BMP-2, thus also showing that the impact of this different anchoring layer could be measured through the whole coating.[44,64]

Keeping these facts in mind, the AFM data showing no pH dependence can be explained as the competitive action of two different phenomena affecting the surface morphology. The first one is the influence of pH on the electrostatic interactions taking place between the polymer chains during the PEM formation, which modifies parameters such as the layers thickness, their entanglement and

eventually the film surface roughness. The second one is the extended influence of the anchoring layer through the whole construct in what could be called a “princess and the pea” phenomenon. As all samples were initially immersed in the same BMP-2 solution for an identical period of time, this first layer is identical for all pH conditions. Looking at the AFM results displayed in Figure 23, this last effect is most probably the dominant one, overpowering even the pH-induced changes in electrostatic bonds, as all surfaces presented the same aspect independently of their assembly pH and no significant variation in surface roughness could be seen when this pH was modified.

VII. Conclusion

BMP-2 – eluting PEMs systems have received much interest from the scientific community in recent years as tailorable coatings designed to enhance the osseointegration of prosthetic implants. However, the medical use of these systems is still hindered by a lack of understanding of their internal structure, controlled release kinetics, stimulus-dependent behavior, and how all of these parameters are linked and interact with each other. The work presented in this report aimed to investigate a PEM formed by an anchoring layer of BMP-2 covered by five PMAA/PLH bilayers, with the goal of determining how its assembly pH would impact its structure and properties.

Different BMP-2 release profiles were obtained for each pH condition, the slower ones being assembled at pH values centered around pH = 6. The initial amount of BMP-2 loaded was estimated to 2 μg/cm², and all pH conditions exhibited a sustained release profile for at least twenty-five days. This system can thus be considered as a suitable implant coating candidate. Further studies at pH = 4 and pH = 5 showed that more than two months of release could be achieved. The profiles obtained for these two pH values were neither in agreement with a Fickian or a Higuchi model, but rather with a power law model. This indicated that the release process was not relying solely on pure diffusion, and probably also involved a mass transport phenomenon due to the dynamic swelling of the multilayer.

The investigation of the PEM formation using QCM-D demonstrated the need to filter the solutions prior to use in order to avoid discrepancies due to polymer conformational transitions. Several trends, related to the mass adsorbed in each layer, could be observed. The most significant ones were an increased mass adsorbed when the assembly pH decreased, a bigger mass of PLH adsorbed by bilayer when compared to PMAA, and the general exponential growth of the PEM. These phenomena were most likely due to the shifting of electrostatic interactions and polymer conformations, both pH-dependent. The pH of the rinsing water was shown to impact the mass adsorbed, too; however the available data was not sufficient for any definite conclusions to be drawn. Nonetheless, the assembly pH appeared to be indeed a critical factor for the PEM internal structure.

Considerations related to the viscoelasticity of the films demonstrated that thin rigid PEMs were formed in most cases, thus allowing for the use of the Sauerbrey theory. However, certain pH conditions might require the use of a viscoelastic model such as the Kelvin-Voigt model in order to obtain a more accurate representation of the assembly process and resulting structure.

The decrease in surface energy as the assembly pH became more basic confirmed that the changes in the internal structure also impacted the PEM surface properties. The modified layer entanglement and influence of underlying layers reflected a shift in the balance of electrostatic interactions caused by the assembly pH. However, the surface topography remained unchanged at different assembly pH values, indicating that the influence of the first anchoring layer was dominating over other interactions that may impact the surface morphology.

Future works should aim to confirm and expand these results to increase the understanding of this promising PEM system. In that regard, complete release profiles should be obtained for all pH conditions in order to assess the potential of this coating for implant applications and obtain reliable percentage data. The results from these experiments could eventually lead to a global model accounting for the pH-dependent release behavior and able to predict it. Similarly, the study of the multilayer formation process should be investigated for other pH conditions in order to confirm the trends presented in this report as well as obtain reliable quantitative data. To do so, determining the polymer molecules conformations depending on the solution pH might be necessary. Finally, as this BMP-2-eluting coating is designed for biological applications, the cell response that the different assembly pH conditions will cause should be considered, especially regarding osteoblasts differentiation and proliferation. These supplementary data, coupled with the ones already investigated in this report, could eventually allow for a tunable implant coating to be precisely designed and controlled in order to efficiently promote osseointegration and improve current prosthetic technologies.

VIII. References

(1) Fingar, K. R.; Stocks, C.; Weiss, A. J.; Steiner, C. A. *Most Frequent Operating Room Procedures Performed in U.S. Hospitals, 2003-2012*; 2014.

(2) Magboo, R.; Peterson, A. M. Encyclopedia of Surface and Colloid Science , Second Edition Polyelectrolyte multilayers for controlled release of biologically relevant molecules. *Encyclopedia of Surface and Colloid Science, Second Edition*.

(3) Bauer, T. W.; Schils, J. *Skeletal Radiol.* **1999**, *28*, 483–497.

(4) Mavrogenis, a. F.; Dimitriou, R.; Parvizi, J.; Babis, G. C. *J. Musculoskelet. Neuronal Interact.* **2009**, *9*, 61–71.

(5) Skirtach, A. G.; Yashchenok, A. M.; Möhwald, H. *Chem. Commun.* **2011**, *47*, 12736.

(6) Quinn, J. F.; Caruso, F. *Langmuir* **2004**, *20*, 20–22.

(7) Cho, C.; Jeon, J. W.; Lutkenhaus, J.; Zacharia, N. S. *ACS Appl. Mater. Interfaces* **2013**, *5*, 4930–4936.

(8) Omura, Y.; Kyung, K.; Shiratori, S.; Kim, S. *Ind. Eng. Chem. Res.* **2014**, 11727–11733.

(9) Schmidt, D. J.; Min, Y.; Hammond, P. T. *Soft Matter* **2011**, *7*, 6637.

(10) Wohl, B. M.; Engbersen, J. F. J. *J. Control. Release* **2012**, *158*, 2–14.

(11) Dorland. In *Dorland's Medical Dictionary for Health Consumers*; Sanders, 2007.

(12) Finch, J. *Lancet* **2011**, *377*, 548–549.

(13) Brand, R. a.; Mont, M. a.; Manring, M. M. *Clin. Orthop. Relat. Res.* **2011**, *469*, 1525–1527.

(14) Caton, J.; Papin, P. *e-mémoires l'Académie Natl. Chir.* **2012**, *11*, 1–7.

(15) OECD. *OECD Publ.* **2013**, 210.

(16) HCUPnet http://hcupnet.ahrq.gov/ (accessed Apr 27, 2015).

(17) Weiss, A. J.; Elixhauser, A.; Andrews, R. M. *Characteristics of Operating Room Procedures in U.S. Hospitals*; Rockville, MD, 2014.

(18) Steiner, C. A.; Andrews, R.; Barrett, M.; Weiss, A. J. *HCUP Projections: Mobility/Orthopedic Procedures 2003 to 2012*; 2012.

(19) Goodman, S. B.; Yao, Z.; Keeney, M.; Yang, F. *Biomaterials* **2013**, *34*, 3174–3183.

(20) Vrana, N. E.; Erdemli, O.; Francius, G.; Fahs, a; Rabineau, M.; Debry, C.; Tezcaner, a; Keskin, D.; Lavalle, P. *J. Mater. Chem. B* **2014**, *2*, 999–1008.

(21) Itoh, Y.; Matsusaki, M.; Kida, T.; Akashi, M. *Biomacromolecules* **2008**, *9*, 2202–2206.

(22) Dierich, A.; Le Guen, E.; Messaddeq, N.; Stoltz, J. F.; Netter, P.; Schaaf, P.; Voegel, J. C.; Benkirane-Jessel, N. *Adv. Mater.* **2007**, *19*, 693–697.

(23) Wang, J.; Guo, J.; Liu, J.; Wei, L.; Wu, G. *Int. J. Mol. Sci.* **2014**, *15*, 10150–10168.

(24) Shah, N. J.; Hyder, M. N.; Quadir, M. a; Dorval Courchesne, N.-M.; Seeherman, H. J.; Nevins, M.; Spector, M.; Hammond, P. T. *Proc. Natl. Acad. Sci. U. S. A.* **2014**, *111*, 12847–12852.

(25) Poth, N.; Seiffart, V.; Gross, G.; Menzel, H.; Dempwolf, W. *Biomolecules* **2015**, *5*, 3–19.

(26) Nath, S. D.; Abueva, C.; Kim, B.; Lee, B. T. *Carbohydr. Polym.* **2015**, *115*, 160–169.

(27) Diefenbeck, M.; Mückley, T.; Schrader, C.; Schmidt, J.; Zankovych, S.; Bossert, J.; Jandt, K. D.; Faucon, M.; Finger, U. *Biomaterials* **2011**, *32*, 8041–8047.

(28) Nayak, S.; Dey, T.; Naskar, D.; Kundu, S. C. *Biomaterials* **2013**, *34*, 2855–2864.

(29) Kim, S. E.; Kim, C.-S.; Yun, Y.-P.; Yang, D. H.; Park, K.; Kim, S. E.; Jeong, C.-M.; Huh, J.-B. *Carbohydr. Polym.* **2014**, *114*, 123–132.

(30) Boura, C.; Menu, P.; Payan, E.; Picart, C.; Voegel, J. C.; Muller, S.; Stoltz, J. F. *Biomaterials* **2003**, *24*, 3521–3530.

(31) Chien, H. W.; Tan, S. F.; Wei, K. L.; Tsai, W. B. *Colloids Surfaces B Biointerfaces* **2011**, *88*, 297–303.

(32) Shukla, A.; Fleming, K. E.; Chuang, H. F.; Chau, T. M.; Loose, C. R.; Stephanopoulos, G. N.; Hammond, P. T. *Biomaterials* **2010**, *31*, 2348–2357.

(33) Meyer, F.; Dimitrova, M.; Jedrzejenska, J.; Arntz, Y.; Schaaf, P.; Frisch, B.; Voegel, J. C.; Ogier, J. *Biomaterials* **2008**, *29*, 618–624.

(34) Lee, I.-C.; Wu, Y.-C. *ACS Appl. Mater. Interfaces* **2014**, *6*, 14439–14450.

(35) Zhang, C.; Hirt, D. E. *Polymer (Guildf).* **2007**, *48*, 6748–6754.

(36) Gand, A.; Hindié, M.; Chacon, D.; van Tassel, P. R.; Pauthe, E. *Biomatter* **2014**, *4*, e28823.

(37) Huang, X.; Zacharia, N. S. *Soft Matter* **2013**, *9*, 7735.

(38) Fakhrullin, R. F.; Zamaleeva, A. I.; Minullina, R. T.; Konnova, S. a.; Paunov, V. N. *Chem. Soc. Rev.* **2012**, *41*, 4189.

(39) Zhang, J.; Chua, L. S.; Lynn, D. M. *Langmuir* **2004**, *20*, 8015–8021.

(40) Moskowitz, J. S.; Blaisse, M. R.; Samuel, R. E.; Hsu, H. P.; Harris, M. B.; Martin, S. D.; Lee, J. C.; Spector, M.; Hammond, P. T. *Biomaterials* **2010**, *31*, 6019–6030.

(41) Shukla, A.; Fuller, R. C.; Hammond, P. T. *J. Control. Release* **2011**, *155*, 159–166.

(42) Shah, N. J.; Macdonald, M. L.; Beben, Y. M.; Padera, R. F.; Samuel, R. E.; Hammond, P. T. *Biomaterials* **2011**, *32*, 6183–6193.

(43) Macdonald, M. L.; Samuel, R. E.; Shah, N. J.; Padera, R. F.; Beben, Y. M.; Hammond, P. T. *Biomaterials* **2011**, *32*, 1446–1453.

(44) Peterson, A. M.; Pilz-Allen, C.; Kolesnikova, T.; Möhwald, H.; Shchukin, D. *ACS Appl. Mater. Interfaces* **2014**, *6*, 1866–1871.

(45) Schönhoff, M.; Ball, V.; Bausch, A. R.; Dejugnat, C.; Delorme, N.; Glinel, K.; Klitzing, R. V.; Steitz, R. *Colloids Surfaces A Physicochem. Eng. Asp.* **2007**, *303*, 14–29.

(46) Sukhishvili, S. A. *Curr. Opin. Colloid Interface Sci.* **2005**, *10*, 37–44.

(47) Schönhoff, M. *Curr. Opin. Colloid Interface Sci.* **2003**, *8*, 86–95.

(48) Glinel, K.; Déjugnat, C.; Prevot, M.; Schöler, B.; Schönhoff, M.; Klitzing, R. V. *Colloids Surfaces A Physicochem. Eng. Asp.* **2007**, *303*, 3–13.

(49) Sato, K.; Yoshida, K.; Takahashi, S.; Anzai, J. I. *Adv. Drug Deliv. Rev.* **2011**, *63*, 809–821.

(50) Gong, R.; Li, C.; Zhu, S.; Zhang, Y.; Du, Y.; Jiang, J. *Carbohydr. Polym.* **2011**, *85*, 869–874.

(51) Chen, S. C.; Wu, Y. C.; Mi, F. L.; Lin, Y. H.; Yu, L. C.; Sung, H. W. *J. Control. Release* **2004**, *96*, 285–300.

(52) Crouzier, T.; Sailhan, F.; Becquart, P.; Guillot, R.; Logeart-Avramoglou, D.; Picart, C. *Biomaterials* **2011**, *32*, 7543–7554.

(53) Guillot, R.; Gilde, F.; Becquart, P.; Sailhan, F.; Lapeyrere, A.; Logeart-Avramoglou, D.; Picart, C. *Biomaterials* **2013**, *34*, 5737–5746.

(54) Pavlukhina, S.; Sukhishvili, S. *Adv. Drug Deliv. Rev.* **2011**, *63*, 822–836.

(55) Antipov, A. A.; Sukhorukov, G. B.; Leporatti, S.; Radtchenko, I. L.; Donath, E.; Möhwald, H. *Colloids Surfaces A Physicochem. Eng. Asp.* **2002**, *198-200*, 535–541.

(56) Antipov, A. A.; Sukhorukov, G. B.; Donath, E.; Möhwald, H. *J. Phys. Chem. B* **2001**, *105*, 2281–2284.

(57) Antipov, A. A.; Sukhorukov, G. B. *Adv. Colloid Interface Sci.* **2004**, *111*, 49–61.

(58) Shivananju, B. N.; Prashanth, G. R.; Asokan, S.; Varma, M. M. *Sensors Actuators, B Chem.* **2014**, *201*, 37–45.

(59) Itano, K.; Choi, J.; Rubner, M. F. *Macromolecules* **2005**, *38*, 3450–3460.

(60) Hiller, J.; Rubner, M. F. *Macromolecules* **2003**, *36*, 4078–4083.

(61) Peterson, A. M.; Möhwald, H.; Shchukin, D. G. *Biomacromolecules* **2012**, *13*, 3120–3126.

(62) Burke, S. E.; Barrett, C. J. *Macromolecules* **2004**, *37*, 5375–5384.

(63) Thompson, M. T.; Berg, M. C.; Tobias, I. S.; Rubner, M. F.; Van Vliet, K. J. *Biomaterials* **2005**, *26*, 6836–6845.

(64) Peterson, A. M.; Pilz-Allen, C.; Möhwald, H.; Shchukin, D. G. *J. Mater. Chem. B* **2014**, *2*, 2680–2687.

(65) Bessegato, G. G.; Guaraldo, T. T.; Zanoni, M. V. B. *Mod. Electrochem. Methods Nano, Surf. Corros. Sci.* **2014**, 271–319.

(66) Marx, K. A. *Biomacromolecules* **2003**, *4*, 1099–1120.

(67) Rickert, J.; Brecht, A; Göpel, W. *Anal. Chem.* **1997**, *69*, 1441–1448.

(68) Notley, S. M.; Eriksson, M.; Wågberg, L. *J. Colloid Interface Sci.* **2005**, *292*, 29–37.

(69) Owens, D. K.; Wendt, R. C. *J. Appl. Polym. Sci.* **1969**, *13*, 1741–1747.

(70) Jalili, N.; Laxminarayana, K. *Mechatronics* **2004**, *14*, 907–945.

(71) Schön, P.; Gosa, M.; Vancso, G. J. *Rev. Roum. Chim.* **2013**, *58*, 577–583.

(72) The Opensource Handbook of Nanoscience and Nanotechnology http://en.wikibooks.org/wiki/Nanotechnology.

(73) Huang, X.; Brazel, C. S. *J. Control. Release* **2001**, *73*, 121–136.

(74) Siepmann, J.; Peppas, N. A. *Adv. Drug Deliv. Rev.* **2001**, *48*, 139–157.

(75) Siepmann, J.; Peppas, N. A. *Int. J. Pharm.* **2011**, *418*, 6–12.

(76) Liu, T. Y.; Lin, Y. L. *Acta Biomater.* **2010**, *6*, 1423–1429.

(77) Berg, M. C.; Zhai, L.; Cohen, R. E.; Rubner, M. F. *Biomacromolecules* **2006**, *7*, 357–364.

(78) Varshosaz, J.; Falamarzian, M. *Eur. J. Pharm. Biopharm.* **2001**, *51*, 235–240.

(79) Garg, A.; Heflin, J. R.; Gibson, H. W.; Davis, R. M. *Langmuir* **2008**, *24*, 10887–10894.

(80) Richert, L.; Arntz, Y.; Schaaf, P.; Voegel, J. C.; Picart, C. *Surf. Sci.* **2004**, *570*, 13–29.

(81) Dixon, M. C. *J. Biomol. Tech.* **2008**, *19*, 151–158.

(82) Janshoff, A.; Galla, H. J.; Steinem, C. *Angew. Chemie - Int. Ed.* **2000**, *39*, 4004–4032.

(83) Samuel, R. E.; Shukla, A.; Paik, D. H.; Wang, M. X.; Fang, J. C.; Schmidt, D. J.; Hammond, P. T. *Biomaterials* **2011**, *32*, 7491–7502.

(84) Aggarwal, N.; Altgärde, N.; Svedhem, S.; Michanetzis, G.; Missirlis, Y.; Groth, T. *Macromol. Biosci.* **2013**, *13*, 1327–1338.

(85) Elzbieciak, M.; Kolasińska, M.; Zapotoczny, S.; Krastev, R.; Nowakowska, M.; Warszyński, P. *Colloids Surfaces A Physicochem. Eng. Asp.* **2009**, *343*, 89–95.

(86) Zankovych, S.; Bossert, J.; Faucon, M.; Finger, U.; Jandt, K. D. *Adv. Eng. Mater.* **2011**, *13*, 454–461.

(87) Kolasińska, M.; Krastev, R.; Warszyński, P. *J. Colloid Interface Sci.* **2007**, *305*, 46–56.

(88) Klitzing, R. V. . *Phys. Chem. Chem. Phys.* **2006**, *8*, 5012–5033.

(89) McAloney, R. A.; Sinyor, M.; Dudnik, V.; Cynthia Goh, M. *Langmuir* **2001**, *17*, 6655–6663.

(90) Koetz, J.; Kosmella, S. *Polyelectrolytes and Nanoparticles*, Springer.; 2007.

(91) Irwin, E. F.; Ho, J. E.; Kane, S. R.; Healy, K. E. *Langmuir* **2005**, *21*, 5529–5536.

(92) Vogt, B. D.; Lin, E. K.; Wu, W.; White, C. C. *J. Phys. Chem. B* **2004**, 12685–12690.

(93) Kanazawa, K. K.; Gordon, J. G. *Anal. Chem.* **1985**, *57*, 1770–1771.

(94) White, C. C.; Schrag, J. L. *J. Chem. Phys.* **1999**, *111*, 11192–11206.

(95) Voinova, M. V.; Rodahl, M.; Jonson, M.; Kasemo, B. *Phys. Scr.* **1999**, *59*, 391–396.

(96) Chien, H. W.; Wu, S. P.; Kuo, W. H.; Wang, M. J.; Lee, C.; Lai, J. Y.; Tsai, W. B. *Colloids Surfaces B Biointerfaces* **2010**, *77*, 270–278.

(97) Lukkari, J.; Salomäki, M.; Ääritalo, T.; Loikas, K.; Laiho, T.; Kankare, J. *Langmuir* **2002**, *18*, 8496–8502.

(98) Peggion, E.; Cosani, A.; Terbojevich, M.; Scoffone, E. *Macromolecules* **1971**, *4*, 725–731.

(99) Castro, P.; Resa, P.; Elvira, L. *IOP Conf. Ser. Mater. Sci. Eng.* **2012**, *42*, 012046.

(100) Nirschl, M.; Schreiter, M.; Vörös, J. *Sensors Actuators, A Phys.* **2011**, *165*, 415–421.

(101) Baba, A.; Kaneko, F.; Advincula, R. C. *Colloids Surfaces A Physicochem. Eng. Asp.* **2000**, *173*, 39–49.

(102) Kelly, P. In *Part I : An Introduction to Solid Mechanics*; The University of Auckland 2013: Auckland, 2013; pp 288–300.

(103) Höök, F.; Kasemo, B.; Nylander, T.; Fant, C.; Sott, K.; Elwing, H. *Anal. Chem.* **2001**, *73*, 5796–5804.

(104) Information on Contact Angle http://www.ramehart.com/contactangle.htm.

(105) Żenkiewicz, M. *J. Achiev. Mater. Manuf. Eng.* **2007**, *24*, 137–145.

(106) Burke, S. E.; Barrett, C. J. *Langmuir* **2003**, *19*, 3297–3303.

(107) Köstler, S.; Delgado, A. V.; Ribitsch, V. *J. Colloid Interface Sci.* **2005**, *286*, 339–348.

(108) Solid surface energy (SFE) for common polymers http://www.surface-tension.de/solid-surface-energy.htm (accessed Mar 31, 2015).

(109) Mhamdi, L.; Picart, C.; Lagneau, C.; Othmane, A.; Grosgogeat, B.; Jaffrezic-Renault, N.; Ponsonnet, L. *Mater. Sci. Eng. C* **2006**, *26*, 273–281.

(110) Gong, X. *Phys. Chem. Chem. Phys.* **2013**, *15*, 10459–10465.

(111) Niepel, M. S.; Peschel, D.; Sisquella, X.; Planell, J. a.; Groth, T. *Biomaterials* **2009**, *30*, 4939–4947.

IX. Appendices

1. OECD data regarding hip and knee replacement procedures

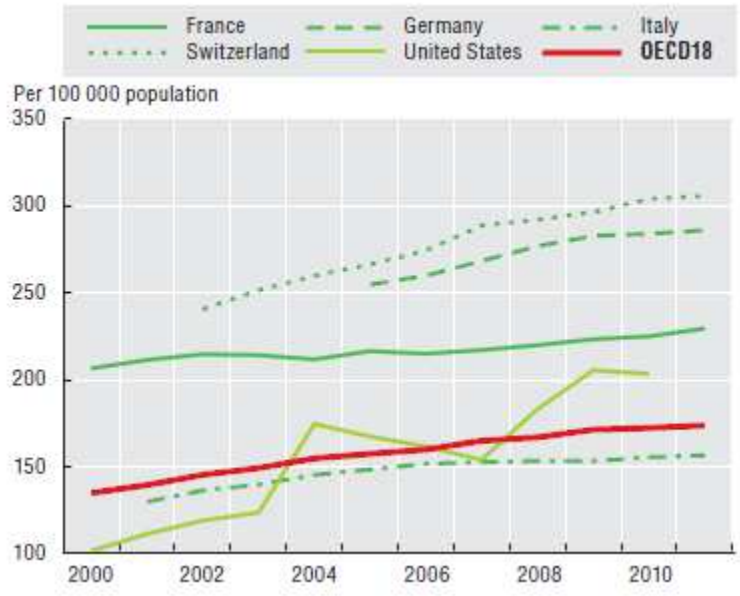

Figure A1: Trend in hip replacement surgery, selected OECD countries, 2000 to 2011 (or nearest year)[15]

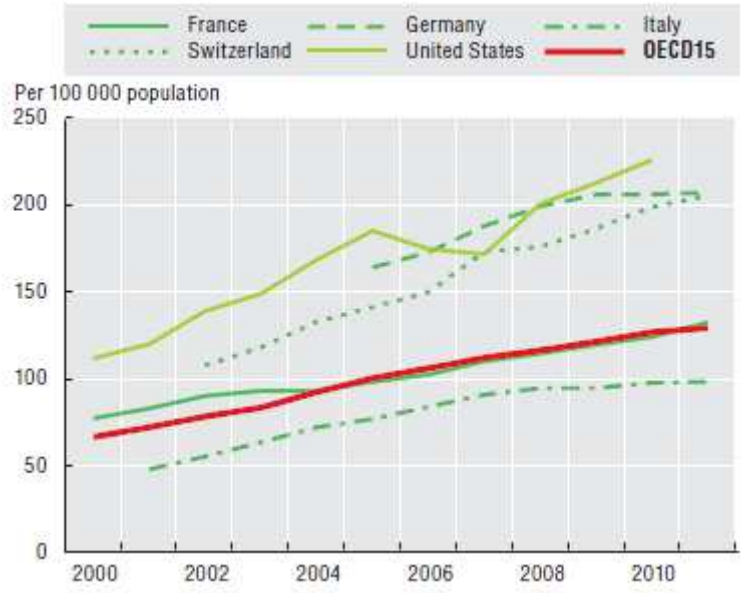

Figure A2: Trend in knee replacement surgery, selected OECD countries, 2000 to 2011 (or nearest year)[15]

2. HCUP data regarding operating room procedures in the United States

Multiple specific procedures (2011)

ICD-9-CM all-listed procedure code and name		Total number of discharges	Standard errors: Total number of discharges
81.51	Total Hip Replacement	293,936	12,042
81.52	Partial Hip Replacement	101,139	2,590
81.53	Revise Hip Replacement (after Oct 1, 2005)	2,422	265
81.54	Total Knee Replacement	618,619	23,106
81.55	Revise Knee Replacement (after Oct 1, 2005)	4,062	353

Multiple specific procedures (2012)

ICD-9-CM all-listed procedure code and name		Total number of discharges	Standard errors: Total number of discharges
81.54	Total Knee Replacement	631,264	12,872
81.55	Revise Knee Replacement (after Oct 1, 2005)	3,130	170

Figure A3: Hip and knee replacement and revision procedures in the U.S.[16]

Rank	All-listed OR procedure*	Number of procedures, in thousands
All-listed OR procedures		**15,662**
1	Cesarean section	1,272
2	Circumcision	1,108
3	Arthroplasty of knee	718
4	Percutaneous coronary angioplasty (PTCA)	560
5	Laminectomy, excision intervertebral disc	525
6	Spinal fusion	488
7	Hip replacement, total and partial	467
8	Cholecystectomy and common duct exploration	449
9	Hysterectomy, abdominal and vaginal	389
10	Colorectal resection	333

Figure A4: Most frequent all-listed operating room (OR) procedures performed in U.S. hospitals, 2011 [17]

Rank	First-listed OR procedure*	Aggregate costs for hospital stays, $ in millions	Mean cost per hospital stay, $	Number of stays, in thousands
First-listed OR procedures		**180,335**	**16,600**	**10,867**
1	Spinal fusion	12,837	27,600	465
2	Arthroplasty of knee	11,317	15,900	711
3	Percutaneous coronary angioplasty (PTCA)	9,730	18,800	517
4	Hip replacement, total and partial	7,962	17,200	464
5	Cesarean section	7,481	5,900	1,269
6	Colorectal resection	6,747	23,400	289
7	Coronary artery bypass graft (CABG)	6,411	38,700	166
8	Heart valve procedures	6,070	53,400	114
9	Cholecystectomy and common duct exploration	5,048	12,600	400
10	Treatment, fracture or dislocation of hip and femur	4,275	16,800	255

Figure A5: Most costly first-listed operating room (OR) procedures performed in U.S. hospitals, 2011 [17]

Rank	Procedure	Stays with OR procedure, n	Rate per 100,000 population
Total stays		**7,958,700**	**2,535.7**
1	Arthroplasty knee	700,100	223.0
2	Percutaneous coronary angioplasty (PTCA)	534,600	170.3
3	Laminectomy, excision intervertebral disc	468,200	149.1
4	Hip replacement, total and partial	468,000	149.1
5	Spinal fusion	450,900	143.6
6	Cholecystectomy and common duct exploration	406,300	129.4
7	Partial excision bone	338,000	107.7
8	Hysterectomy, abdominal and vaginal	312,100	99.4
9	Colorectal resection	305,900	97.4
10	Excision, lysis peritoneal adhesions	305,800	97.4

Figure A6: Operating room procedures performed most frequently during hospital stays, 2012 [1]

Measure	Projected Annual Total Discharges for All Adults 2012	Change from 2003 to 2012 Projection for All Adults		
		Total Discharges	Average Total Hospital Cost	Average Length of Stay
primary hip replacement for any reason	427,946	↑	↑	↓
primary hip replacement for osteoarthritis	285,354	↑	↑	↓
primary hip replacement for hip fracture	101,846	—	↑	↓
hip replacement revision surgery	47,024	↑	↑	↓
primary knee arthroplasty for osteoarthritis	675,359	↑	↑	↓
knee replacement revision surgery	60,803	↑	↑	↓
spinal fusion for back problems	347,422	↑	↑	—

Figure A7: Projected annual estimates in 2012 for mobility/orthopedic procedures in U.S. hospitals [18]

3. Salt concentration calculations

The calculations shown here aim to help the reader understand the methodology behind the determination of solution salt concentration. The data used were issued from actual experiments. After measurements, the volume of one drop was determined to be approximately 0.010 mL.

Adjustement of rinsing water to pH = 7

V_{water} = 0.5 L

Addition of 3 drops of NaOH, 0.1 M, and 26 drops of NaOH, 0.01 M.

Total amount of NaOH added:

$$n_{NaOH} = \sum p.C_{NaOH}.V_{drop} = 3 \times 0.1 \times 0.010 \times 10^{-3} + 26 \times 0.01 \times 0.010 \times 10^{-3} = 5.6 \times 10^{-6}\ mol \quad (15)$$

With p the number of drops. From it, the concentration of sodium ions can be found:

$$C_{Na^+} = C_{NaOH} = \frac{n_{NaOH}}{V_{water} + \sum p.V_{drop}} = \frac{5.6 \times 10^{-6}}{0.5 + 29 \times 0.010 \times 10^{-3}} = 1.12 \times 10^{-5} M \quad (16)$$

Adjustement of rinsing water to pH = 6

V_{water} = 0.5 L

Addition of 9 drops of NaOH, 0.01 M.

Total amount of NaOH added:

$$n_{NaOH} = \sum p.C_{NaOH}.V_{drop} = 9 \times 0.01 \times 0.010 \times 10^{-3} = 9 \times 10^{-7}\ mol \quad (17)$$

Concentration of sodium ions:

$$C_{Na^+} = C_{NaOH} = \frac{n_{NaOH}}{V_{water} + \sum p.V_{drop}} = \frac{9 \times 10^{-7}}{0.5 + 9 \times 0.010 \times 10^{-3}} = 1.80 \times 10^{-6} M \quad (18)$$

Amount of salt needed to obtain identical salt concentrations at both pH conditions:

Difference in sodium ions amount:

$$\Delta n_{Na^+} = \Delta n_{NaOH} = n_{NaOH,pH=7} - n_{NaOH,pH=6} = 5.6 \times 10^{-6} - 9 \times 10^{-7} = 4.7 \times 10^{-6} mol \quad (19)$$

As sodium chloride salt NaCl accounts for two charges per molecule upon dissociation (Na^+ and Cl^-), the amount of salt that should be added to the solution at pH = 6 in order to equalize salt concentrations is:

$$n_{NaCl} = \frac{\Delta n_{Na^+}}{2} = \frac{4.7 \times 10^{-6}}{2} = 2.35 \times 10^{-6}\, mol \quad (20)$$

Which represents a mass of salt of:

$$m_{NaCl} = n_{NaCl} \times M_{NaCl} = 2.35 \times 10^{-6} \times 58.44 = 1.37 \times 10^{-4} g \quad (21)$$

This order of mass was so small that it could not be physically measured with the material available, and was considered to be negligible.